Geological Society, London, Memoirs

Chapter 10 The effect of topography on ash-cloud surge generation and propagation

Sarah E. Ogburn, Eliza S. Calder, Paul D. Cole and Adam J. Stinton

Geological Society, London, Memoirs 2014, v.39; p179-194.
doi: 10.1144/M39.10

Notes

Chapter 10

The effect of topography on ash-cloud surge generation and propagation

SARAH E. OGBURN[1]*, ELIZA S. CALDER[1,2], PAUL D. COLE[3,4] & ADAM J. STINTON[3,4]

[1]*Department of Geology, 411 Cooke Hall, State University of New York at Buffalo, Buffalo, NY 14260, USA*

[2]*School of Geosciences, University of Edinburgh, Edinburgh, UK*

[3]*Montserrat Volcano Observatory, Flemmings, Montserrat, West Indies*

[4]*Seismic Research Centre, The University of the West Indies, St Augustine, Trinidad & Tobago, West Indies*

**Corresponding author (e-mail: seogburn@buffalo.edu)*

Abstract: The relationship between valley morphology and ash-cloud surge development for 12 pyroclastic density currents (PDCs) at Soufrière Hills Volcano (SHV), Montserrat is investigated. Channel slope, sinuosity and cross-sectional area were measured from high-resolution digital elevation models (DEMs) using geographical information system (GIS) software; and were compared to geometric parameters of the deposits. The data illustrate three surge-generation regimes: a proximal area of rapid expansion; a medial deflation zone; and a steadier distal surge 'fringe'. The extent to which these regimes develop varies with flow volume. For larger flows, within the proximal and medial regimes, a strong inverse correlation exists between surge detachment and valley cross-sectional area. Surge detachment is also correlated with observed and modelled flow velocities. Areas of topography-induced increases in velocity are interpreted to result in more pervasive fragmentation and fluidization, and thus enhanced surge generation. Distally, surge deposits appear as fringes with decaying extents, indicative of more passive expansion and decreasing velocity. The results indicate that surge mobility and detachment are a complex product of flow mass flux and topography, and that future efforts to model dense–dilute coupled flows will need to account for and integrate several mechanisms acting on different parts of the flow.

The development and subsequent decoupling of dilute, turbulent ash-cloud surges from dense basal pyroclastic flows is poorly understood, unpredictable and often results in deadly consequences. Ash-cloud surges can have a significant lateral component of motion, and have been known to detach and move independently from their parent flows (Fisher 1995). For example, decoupled pyroclastic surges were responsible for fatalities at Mt Pelée, Martinique in 1902 (Fisher & Heiken 1982); Unzen, Japan on 3 June 1991 (Yamamoto *et al.* 1993); at Soufrière Hills Volcano (SHV), Montserrat on 25 June 1997 (Loughlin *et al.* 2002*a*, *b*); and at Merapi Volcano, Indonesia on 18–19 December 1930, 22 November 1994 and October–November 2010 (Bourdier & Abdurachman 2001; Smithsonian Institution 2011; Jenkins *et al*. 2013). Several of these events, and their resultant deposits, have been well described and their dynamics analysed in detail retrospectively. However, it remains the case that a more generalized understanding of how such dense–dilute coupled flows behave and propagate given an array of likely eruption scenarios and terrain characteristics is still beyond our capabilities.

A variety of geophysical flow models exist for simulating the dense concentrated parts of pyroclastic density currents (PDCs) (Sheridan *et al.* 2004; Kelfoun & Druitt 2005; Patra *et al.* 2005; Kelfoun *et al.* 2009) or for simulating the dilute ash-cloud surges (Ishimine 2005). However, because these models use simplified rheological laws that capture the bulk flow behaviour, they cannot model the dense basal avalanches and ash-cloud surges as a coupled dense–dilute system. Complex multiphase models that capture the dynamics of both the turbulent fluid and the intergranular interactions within PDCs have the potential to model the decoupling of surges (e.g. Takahashi & Tsujimoto 2000; Todesco *et al.* 2002; Dartevelle *et al.* 2004; Valentine *et al.* 2011), but these models are computational expensive and, as such, are currently impractical for use in many hazard mapping applications.

In contrast, mapping tools based on simplified empirical relationships, such as LAHARZ or PYROFLOW, have shown success (Wadge *et al.* 1998; Wadge 2009; Widiwijayanti *et al.* 2008) at both simulating the expected inundation from dense basal avalanches and, to a first order, delineating the probable ash-cloud surge extent. These models have the advantage of being computationally simple, making them more suitable for use in hazard mapping during ongoing volcanic crisis. Several simple methods have been employed to estimate the ash-cloud surge delineation. Widiwijayanti *et al.* (2008) used a horizontal buffer of uniform distance applied to the modelled dense basal avalanche. The buffer distance was determined by statistically analysing mapped deposits, and setting the buffer distance equal to 90 (700 m wide) and 50% (500 m wide) confidence limits. Wadge *et al.* (1998), Wadge (2009) and Widiwijayanti *et al.* (2008) also employed a simple one-dimensional (1D) model for lateral motion of the ash-cloud surge from the dense basal avalanche. The model considers the sedimentation of clasts and entrainment of air as the surge moves laterally away from the dense basal avalanche; therefore the limits of surge inundation are drawn where the bulk density of the surge falls below that of ambient air. They do not, however, capture the complex physics associated with flow emplacement, and, in cases where they have been applied, the need for improved reliability in delineating ash-cloud surge inundation has been highlighted (SAC 2007).

Our understanding of these coupled flows remains very incomplete. For development of dense–dilute coupled geophysical models, the key processes to be incorporated can be guided by observed field relationships between dense basal avalanches, ash-cloud surges and topography. A number of field studies investigate the morphology and granulometry of single events in great detail (e.g. Loughlin *et al.* 2002*b*; Charbonnier & Gertisser 2008; Komorowski *et al.* 2010; Lube *et al.* 2011; Komorowski *et al.* 2013), but few aggregate many events in order to extract general information and investigate similarities and differences between PDCs. Complex field relationships that result from the spatial and temporal variability of PDCs need to be reliably distilled in order to understand key physical processes which *apply generically* and which can be incorporated into dense–dilute coupled

From: Wadge, G., Robertson, R. E. A. & Voight, B. (eds) 2014. *The Eruption of Soufrière Hills Volcano, Montserrat from 2000 to 2010.* Geological Society, London, Memoirs, **39**, 179–194. http://dx.doi.org/10.1144/M39.10

Table 10.1. *DEM specifications*

DEM date	Grid spacing	Vertical resolution	Coverage	Source	Notes	Reference
Pre-eruption	10 m	10 m per 25 m^2	Whole	1:25 000 topographical map	Digitized from map	Wadge & Isaacs (1988)
1999	10 m	10 m per 25 m^2	Whole	Terrestrial LiDAR, GPS	Pre-eruption DEM amended with surveys	Wadge (2000)
2007	10 m	7 m per 100 m^2	Whole	Terrestrial LiDAR, GPS	Pre-eruption DEM amended with surveys	R. Herd (unpublished); G. Wadge (unpublished); Ogburn (2008); Darnell *et al.* (2010); SAC (2011)
2010	1 m	15 cm per 1 m^2	Partial	Airborne LiDAR		Cole *et al.* (2010); SAC (2011)

LiDAR, Light Detection and Ranging.

models. In this work, we characterize the effect of topography on PDC deposit distribution, with the objective of gleaning a better understanding of ash-cloud surge-generation and detachment mechanisms associated with block-and-ash flows (BAFs) from lava-dome collapse. Our work addresses the need to extract generic relationships by comparing the ash-cloud surge-inundation patterns of several events, a number of which actually inundate the same drainage systems. Commonalities between these events in the same drainage provide the framework for a generic topography-based model, while discrepancies between the events observed here highlight the important role of PDC volume and/or mass flux. It is envisaged that the relationships found here can be utilized to inform models that deal with ash-cloud surge generation, ranging from those that involve complex geophysics to those that are empirically based.

Previous work

First, we clarify our use of terminology: PDCs are understood to be density-stratified currents (Valentine 1987), which, to varying degrees, develop high concentration, dense undercurrents (pyroclastic flows or dense basal avalanches) and dilute, turbulent, overriding ash clouds (pyroclastic surges or ash-cloud surges). PDCs may form from lava dome collapses, such as at Unzen (Yamamoto *et al.* 1993; Fujii & Nakada 1999), and Merapi (Voight *et al.* 2000; Bourdier & Abdurachman 2001); from column collapses, such as at Mount Vesuvius, Italy (Bullard 1962; Lirer *et al.* 1973); or from directed blasts as at Mount St Helens, Washington, USA (Kieffer 1981; Moore & Sisson 1981); and the Boxing Day event at SHV (Sparks *et al.* 2002; Voight *et al.* 2002). This work largely deals with PDCs generated

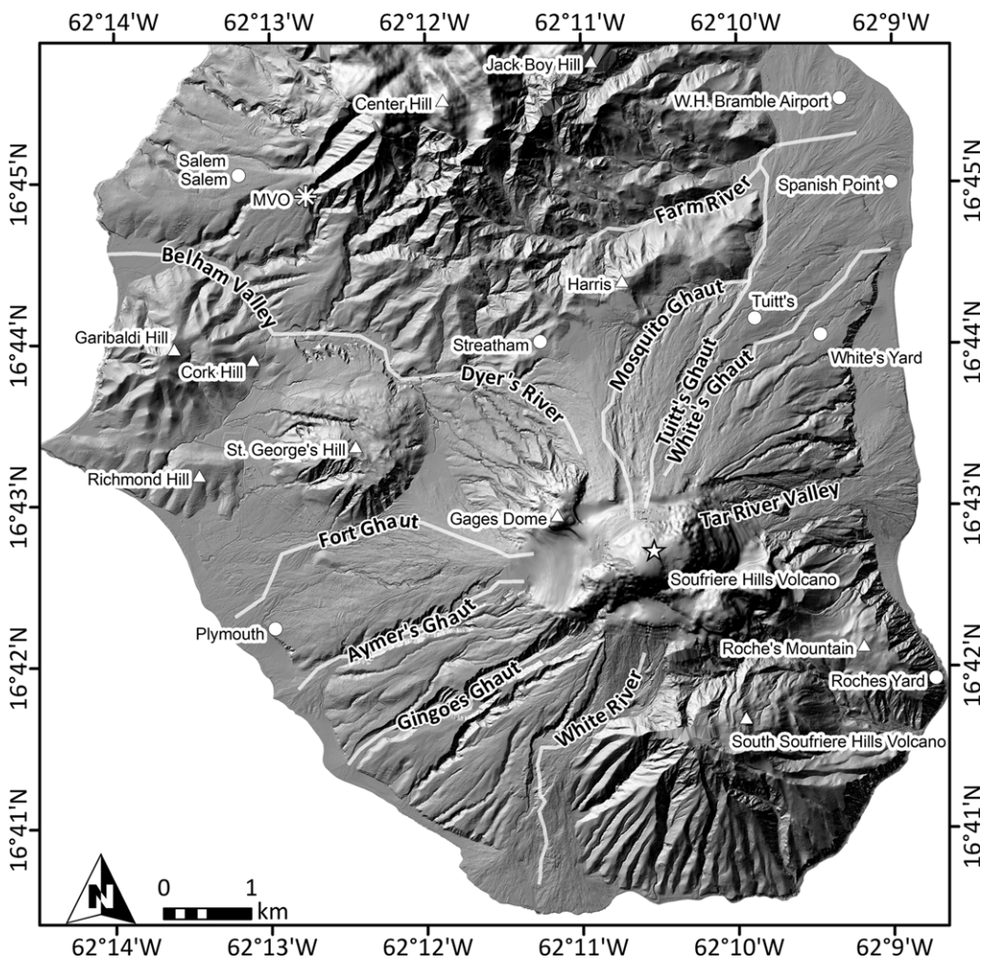

Fig. 10.1. Location map of Montserrat showing valleys measured in this study along with other geographical features, such as the MVO. The base map is a hill-shade of the 2010, 1 m, DEM overlain on the 1999, 10 m, DEM (northern section of the island, lighter grey) both using WGS84 UTM20N.

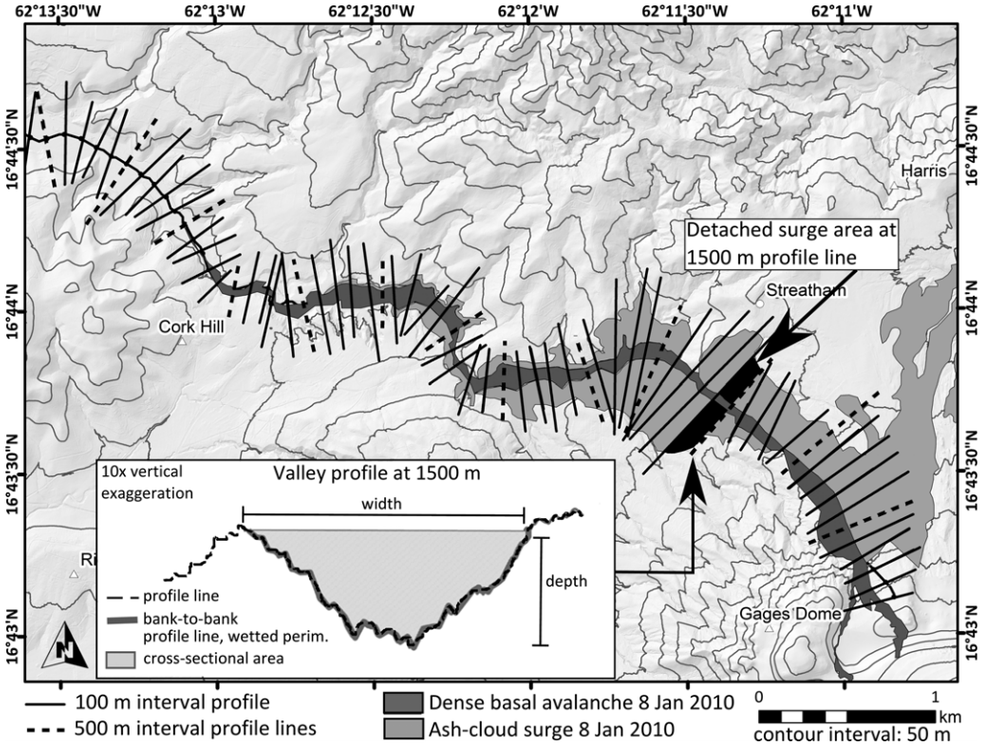

Fig. 10.2. Methodology for measuring valley-latitudinal cross-sectional profiles, and BAF widths and areas for the Belham Valley using the 2010, 1 m, DEM. Cross-sectional profiles were extracted every 100 m (dashed profiles = 500 m), with the inset showing a representative cross-sectional profile. BAF widths were measured across the 100 m profile lines used to measure the underlying channels (black solid and dashed lines). Areas were measured by dividing the BAF into segments using the profile lines, and measuring the area of each segment between the profile lines. The black box shows the detached surge area measured for the 1500 m profile line.

by lava-dome collapse, but also includes two events that are, to some degree, transitional and include an explosive component. Thus, we refer to the high concentration undercurrent as the dense basal avalanche and the overriding dilute component as the ash-cloud surge. We also use the term BAF to refer to the entire PDC generated from lava-dome collapse; this encompasses both the dilute and dense components. The detached pyroclastic surge area is the area inundated by the ash-cloud surge outside the footprint covered by the dense basal avalanche. The total ash-cloud surge area is thus the area covered by the dense basal avalanche plus the detached pyroclastic surge area.

A number of processes have been proposed to contribute to the generation of ash-cloud surges and these include: (1) elutriation of fine particles and gas from the basal avalanche (Fisher 1979; Wilson 1980); (2) entrainment of ambient air into the flow and subsequent thermal expansion of the mixture (McTaggart 1960; Sparks 1976; Wilson & Walker 1982); (3) particle collision and disintegration (comminution and release of gas from pressurized clasts) (Sparks *et al.* 1978; Fujii & Nakada 1999; Dufek & Manga 2008); (4) turbulent diffusion across a boundary layer (Denlinger 1987; Burgisser & Bergantz 2002); and (5) explosive decompression of the pressurized dome (Woods *et al.* 2002). Conversely, Doyle *et al.* (2008) modelled dense basal avalanches as developing out of dilute currents through mass transfer by sedimentation to the base of the current. With respect to ash-cloud surge generation specifically associated with BAFs, several studies (Ishida *et al.* 1980; Denlinger 1987; Fujii & Nakada 1999) have proposed models with an intermediate fluidization zone between the dense basal avalanche and the ash-cloud surge. Ash-cloud surge generation is thus considered within a framework of particle transport (by upwards gas flow or interparticle collisions) from the basal avalanche into the intermediate fluidization zone, followed by the subsequent turbulent suspension of fluidized particles into the ash-cloud surge.

Decoupling of pyroclastic surges has been well documented and a range of behaviour noted. Ash-cloud surges are known to detach and overrun dense basal avalanches after traversing a break in slope, as at Mount Ngauruhoe, New Zealand (Nairn & Self 1978), Santiaguito Volcano, Guatemala (Rose *et al.* 1977), and Merapi (Bourdier & Abdurachman 2001; Lube *et al.* 2011; Jenkins *et al.* 2013). Surges may separate from valley-confined flows when steep topography or barriers are encountered, as was

Table 10.2. *Characteristics of channels. Values are averaged along the length of the channel*

Valley name	DEM date	DEM grid spacing	Average slope (°)	Length (km)	Average cross-sectional area (m^2)	Average depth (m)	Average width (m)	Sinuosity	No. of flows
TRV	1995	10 m	10.17	2.837	41066.8	88.76	706.73	1.09	3
MG	1995	10 m	4.24	7.483	5182.5	37.58	280.05	1.39	2
TG	1995	10 m	7.34	6.528	5092.2	41.32	244.22	1.21	2
WRV	1995	10 m	5.72	5.001	28450.9	91.99	509.28	1.22	2
BV	1995	10 m	5.64	7.338	12679.8	46.58	443.56	1.22	1
BV	2007	10 m	5.40	7.790	9709.8	40.68	401.59	1.19	1
BV	2010	1 m	5.98	7.790	4545.5	21.67	315.57	1.19	1

TRV, Tar River Valley; WRV, White River Valley; TG, Tuitt's Ghaut; MG, Mosquito Ghaut; BV, Belham Valley.

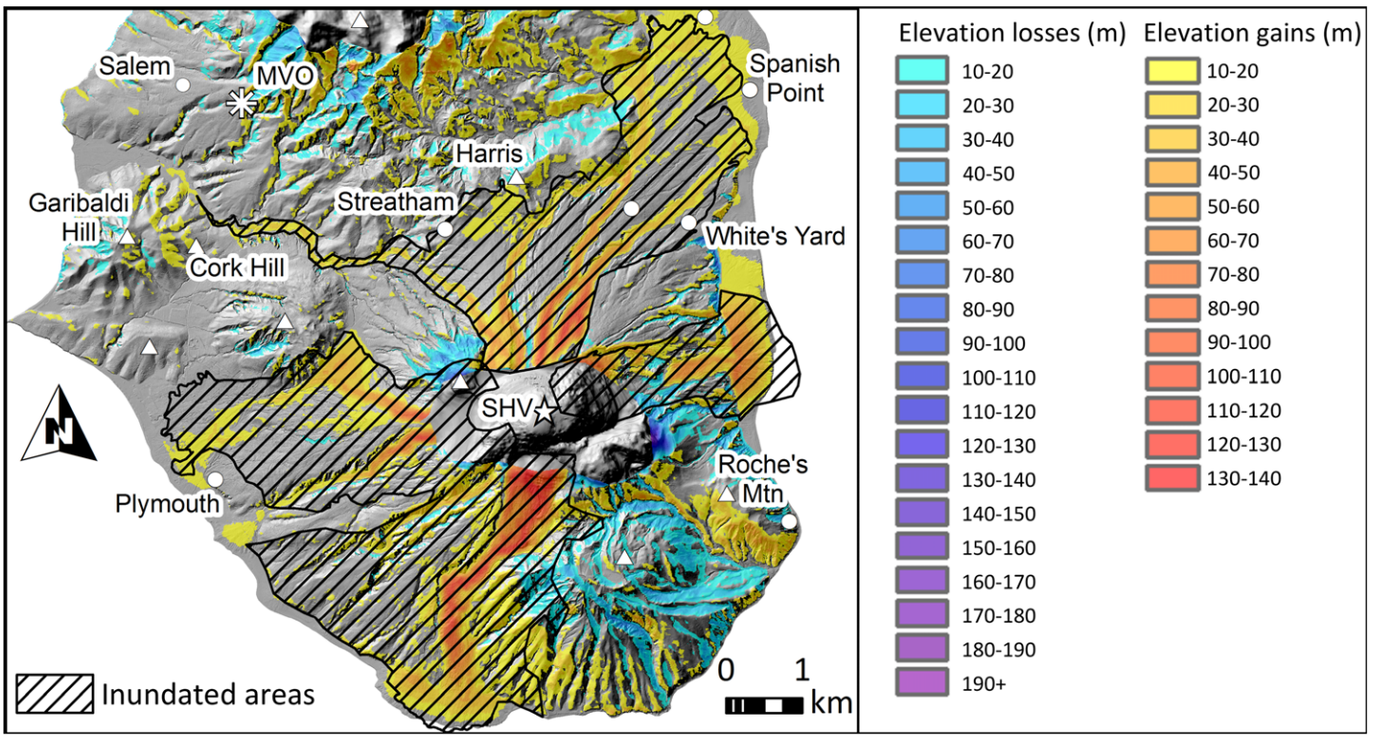

Fig. 10.3. Elevation changes between 1995 and 2010. Yellows–reds indicate elevation gained (deposition) and blues–purples indicate elevation lost (erosion). The hashed areas are those inundated by PDCs. Changes less than 10 m have been excluded to account for georeferencing and grid spacing errors. Proximally, radical elevation changes may be related to the growth or removal of the dome itself and not deposition or erosion by PDCs.

the case for El Chichon Volcano, Mexico (Sigurdsson *et al.* 1987) and at Merapi in 2010 when PDCs encountered ridges (Komorowski *et al*. 2013) and lahar containment structures (Sabo dams) (Charbonnier & Gertisser 2011; Lube *et al*. 2011; Charbonnier *et al*. 2013; Jenkins *et al*. 2013; Komorowski *et al*. 2013). Ash-cloud surges have also been known to overspill narrow channels, especially around valley bends, as at Merapi (Bourdier & Abdurachman 2001; Charbonnier & Gertisser 2008, 2011; Lube *et al.* 2011; Charbonnier *et al*. 2013; Jenkins *et al*. 2013; Komorowski *et al*. 2013), Unzen (Yamamoto *et al.* 1993; Fujii & Nakada 1999) and SHV (Loughlin *et al.* 2002*b*).

For the 25 June 1997 SHV BAF described in detail by Loughlin *et al.* (2002*b*), detachment of ash-cloud surges was found to occur at valley bends and constrictions, and was related to the slope of the channel, and was enhanced by depositional filling. Cole *et al.* (2002), analysing data collated from 14 SHV flows, found

Table 10.3. *Pyroclastic density currents 1996–2010*

Date	Valley	Sustained (S) or discrete (D)	Length[¶] (km)	H/L	Total volume ($\times 10^6$ m^3)	Pf vol. ($\times 10^6$ m^3)	Surge volume ($\times 10^6$ m^3)	Pf area (km^2)	Detached surge area (km^2)
3 April 1996[*]	TRV	D	1.63	0.363	0.2	0.152	0.048	0.096	0.110
12 May 1996[*]	TRV	D	2.95	0.309	0.4	0.331	0.069	0.233	0.197
30 March 1997[*]	WRV	S	4.36	0.190	2.6			0.168	0.129
31 March 1997[*]	TRV	D	2.53	0.340	0.3	0.163	0.137	0.176	0.608
11 April 1997[*]	WRV	S	4.64	0.194	3.0	2.90	0.100	0.403	0.141
5 June 1997[*]	TG	D	3.21	0.268	0.4	0.375	0.025	0.146	0.078
17 June 1997[*]	MG	D	3.83	0.224	0.8	0.766	0.034	0.181	0.103
25 June 1997[*]	MG	S	7.26	0.139	6.4	5.538	0.791	0.906	2.973
21 September 1997[*]	TG	S	6.72	0.137	14.3	13.563	0.737	2.443	2.572
8 January 2007[†]	BV	S	5.70	0.169	4.5			0.501	1.072
2 January 2009[‡]	BV	D	3.47	0.279	0.4–0.6[**]			0.300	0.314
8 January 2010[§]	BV	D	6.62	0.166	1.3[††]			0.445	1.008

TRV, Tar River Valley; WRV, White River Valley; TG, Tuitt's Ghaut; MG, Mosquito Ghaut; BV, Belham Valley.
[*]All PDC information from Calder *et al*. (1999) and Cole *et al*. (2002) except where otherwise noted.
[†]Hards *et al*. (2008); Loughlin *et al*. (2010).
[‡]Komorowski *et al*. (2010).
[§]Cole *et al*. (2014).
[¶]Note: Along-flow length measurements from ArcGIS may differ slightly from other recorded length measurements.
[**]Estimated from run-out using the method from Calder *et al.* (1999).
[††]The 8 January 2010 flow entered several other valleys and had a total volume of 3.4×10^6 m^3.

that there was no evident relationship between the percentage area covered by the detached ash-cloud surge deposit and the total volume of the BAF deposit; that is, large-volume BAFs did not necessarily produce relatively more extensive surge deposits than did small-volume flows. In view of this, surge development and extent was attributed to variations in topographical effects, temperature and dome pore pressure. Steep valley slopes were suggested to enhance air entrainment, resulting in the heating and thermal expansion of the surge cloud, and valley volume capacity was related to the ability of channels to contain the ash-cloud surges. High pore pressures in collapsing dome rock sourced from deep within the dome (as opposed to the collapse of degassed dome carapace) have been invoked by a number of authors to explain surge development by generating large quantities of fine ash (e.g. at Unzen, Sato *et al.* 1992; at Merapi, Bourdier & Abdurachman 2001; Komorowski *et al*. 2013; and at SHV, Cole *et al.* 2002; Loughlin *et al.* 2002*b*; Woods *et al.* 2002). However, at Merapi, surge detachment was also shown to be highly volume-dependent, with large-volume, long-runout BAFs most likely to produce detaching surge clouds (Bourdier & Abdurachman 2001). Analysis of ash-cloud surge detachment from BAFs during the June 2006 eruption at Merapi showed a more passive channel overflow process controlled primarily by valley cross-sectional area, rate of channel confinement (the change in cross-sectional area with distance) and channel sinuosity (Lube *et al.* 2011). Lahar containment structures, known as Sabo dams, were shown to decrease the carrying capacity of channels and to encourage flow avulsion during the 2006 and 2010 Merapi eruptions (Charbonnier & Gertisser 2008, 2011; Lube *et al.* 2011; Charbonnier *et al*. 2013; Jenkins *et al*. 2013). During the 2010 eruption at Merapi, lethal surge detachment occurred even at the most distal reaches of large-volume, long-runout flows (16 km), although the decoupled surges were relatively low energy and low turbulence because of the effects of upstream valley constrictions (Smithsonian Institution 2011; Jenkins *et al*. 2013; Komorowski *et al*. 2013).

Valley morphology

Using GIS software in conjunction with digital elevation models (DEMs) allows for the rapid, precise and reproducible measurement of channel morphology. Multiple DEMs exist for the island of Montserrat, with horizontal spacings of 1–10 m and vertical resolutions of 15 cm–10 m (Table 10.1) (Wadge & Isaacs 1988; SAC 2011). GIS tools allow for the precise and hydrologically correct delineation of stream networks, as well as true 'path-length' measurements that fully account for sinuosity and elevation changes. Five primary drainage systems were investigated in this work (Fig. 10.1): the Belham Valley, Mosquito Ghaut, Tuitt's Ghaut, the Tar River Valley and the White River Valley. Longitudinal valley thalweg profiles were extracted for each drainage, with average valley slopes ranging from about 4 to 10°. A series of latitudinal (cross-sectional) profiles measured at 100 m intervals were also collected for each valley (Fig. 10.2). The cross-sectional profiles were drawn with intentionally liberal lengths (0.5–1 km) in order to fully capture the geometry of adjacent channel banks. While these cross-sectional profiles appear to intersect in Figure 10.2, the actual profile data were limited during processing to only include the bank-to-bank profile information. Valley depth, width, wetted perimeter, cross-sectional area and sinuosity were measured for each profile. A summary of the average valley characteristics can be found in Table 10.2. The Tar River Valley is the steepest, with an average slope of 10°, and also broadest, but it is relatively straight (low sinuosity). The Belham Valley, of particular importance for hazard management because of its proximity to an inhabited residential zone and the Montserrat Volcano Observatory (MVO), is relatively long, sinuous and shallow, with an average slope of only 5–6°.

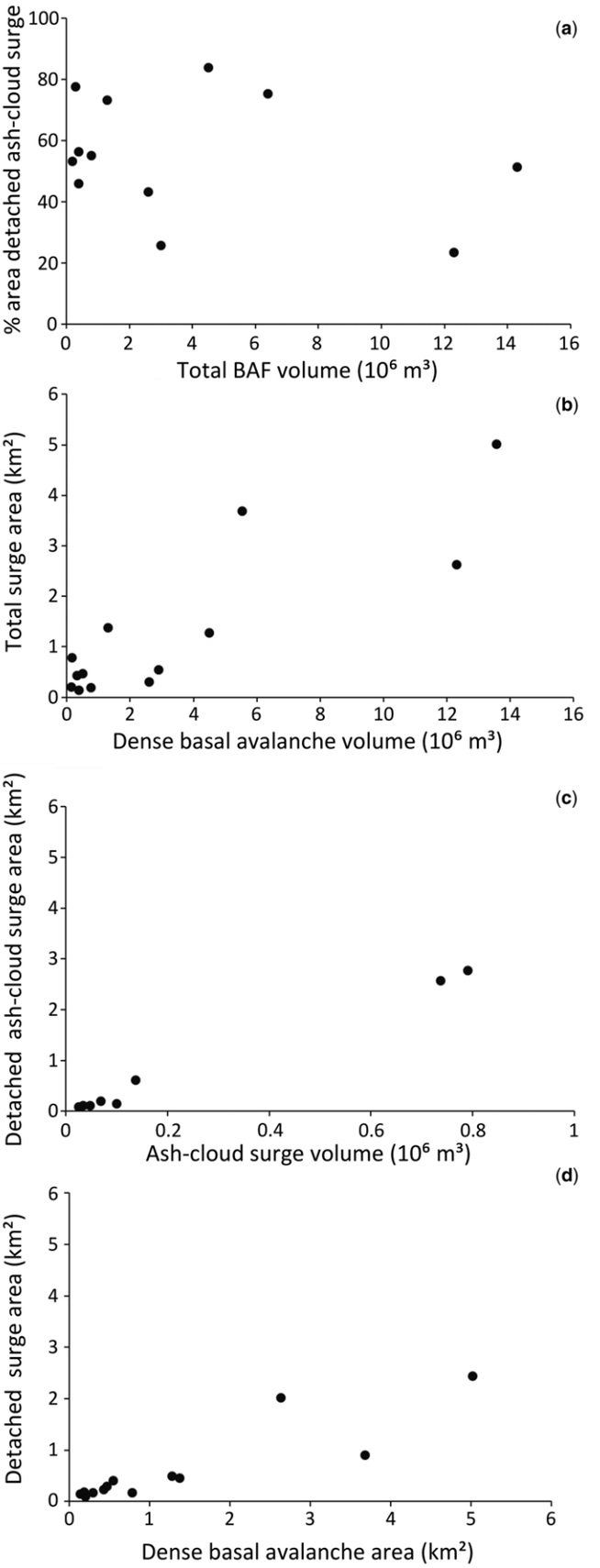

Fig. 10.4. (**a**) Plot of total BAF volume v. the percentage area of detached ash-cloud surge (after Cole *et al.* 2002). (**b**) Total surge area v. dense basal avalanche volume. (**c**) Detached surge area v. ash-cloud surge volume. (**d**) Detached surge area v. dense basal avalanche area.

Temporal changes

By comparing DEMs from different periods, it is possible to identify areas of time-averaged erosion or deposition. Elevation gains (deposition) and losses (erosion) over the last 15 years can be seen in Figure 10.3. While small geolocation errors result in minor gains and losses appearing over the entire map, it is obvious that areas inundated by PDCs (the hashed region in Fig. 10.3) have experienced net gains of as much as 100–140 m in elevation due to deposition, especially in proximal areas. The formation of new coastline is also apparent, especially where the Tar River Valley, Tuitt's Ghaut and the White River Valley reach the sea. Topographical changes during an ongoing eruptive crisis can have important hazard implications, as in-filled valleys are less able to contain subsequent flows and steeper average drainage slopes can increase flow mobility. These changes are also important to note for modelling purposes. Many mass-flow models simulate flows over natural terrain using DEMs, and the uncertainty due to the DEM collection method, interpolation method, resolution and post-DEM topography changes should be considered (e.g. Darnell *et al.* 2010; Stefanescu *et al.* 2010*a*, *b*).

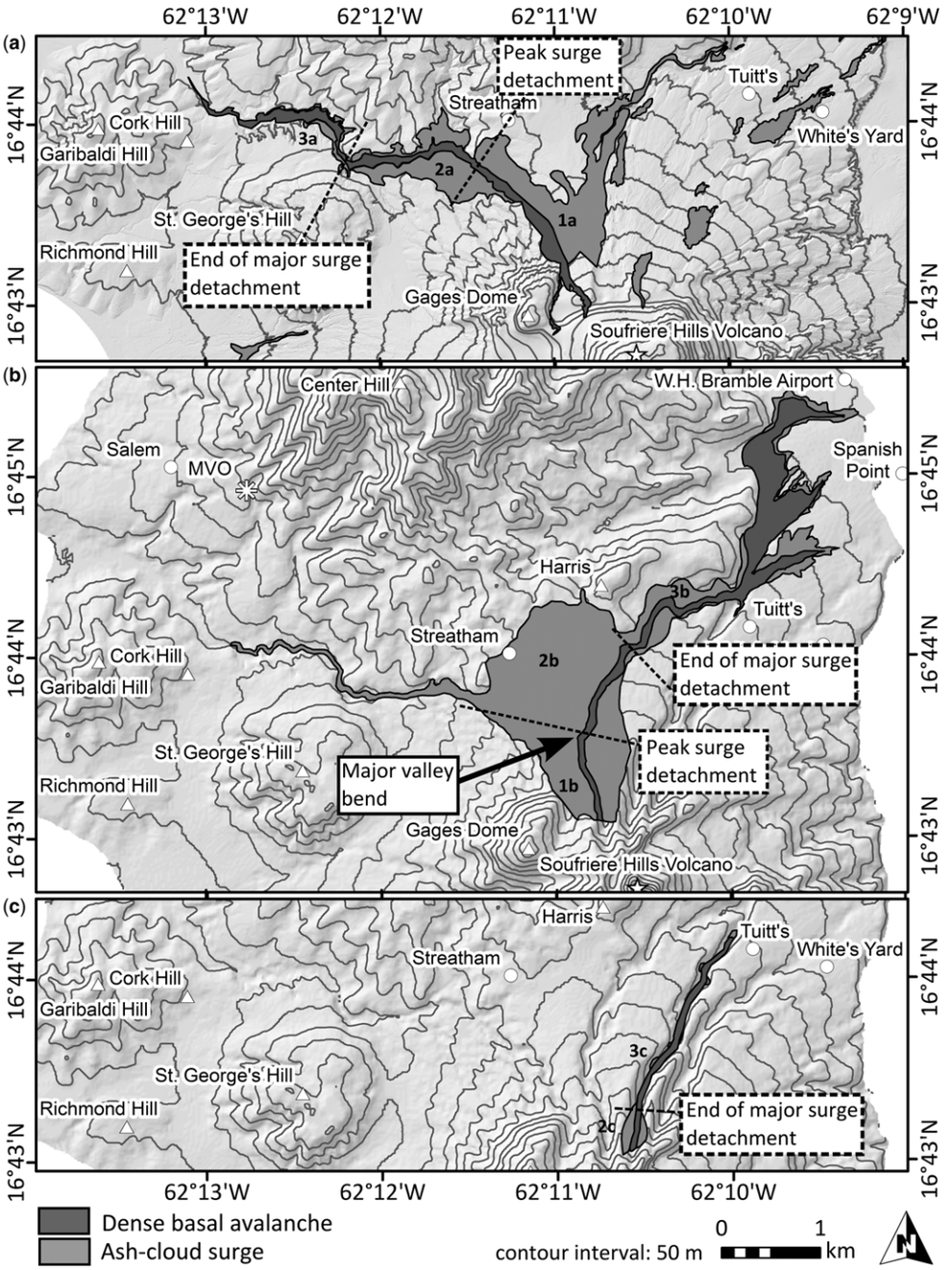

Fig. 10.5. (**a**) 8 January 2010 BAF deposit overlain on the 2010, 1 m, DEM. The surge deposit detaches and spills out of the channel for the first 3100 m, expanding rapidly in the proximal region (1a), declining in the medial region (2a), then appearing only as a fringe around the dense basal avalanche deposit in the distal region (3a). (**b**) 25 June 1997 BAF deposit overlain on the 1995, 10 m, DEM. The surge deposit detaches and spreads to the NE, away from the dense basal avalanche deposit. In the proximal (1b) and medial (2b) zones, the surge was powerful enough to fell trees. After approximately 2700 m, the surge appears only as a fringe (3b) and trees remain standing. *Note*: the small surge-derived flow in the Belham Valley was not included in measurements. (**c**) 5 June 1997 BAF deposit overlain on the 1995, 10 m, DEM. The surge deposit detaches only in the proximal 500 m, and begins declining immediately (2c). Distally (3c), there is minimal surge detachment around bends.

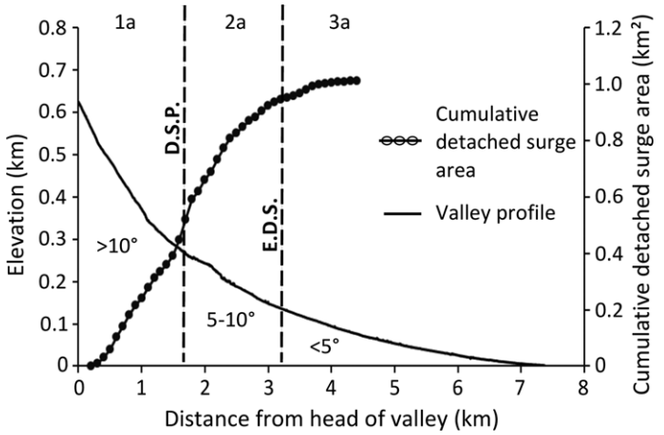

Fig. 10.6. The relationship between cumulative detached surge area and channel slope using the 8 January 2010 BAF as an example. The proximal region of vigorous surge detachment and expansion (1a) corresponds to slopes >10°, with the peak surge detachment (D.S.P.) occurring on slopes around 10°. In the medial region (2a), the surge detachment decreases expansion on slopes from 5 to 10°. The distal region (3a), where the surge exists as a narrow fringe, correspond to slopes <5°. D.S.P., detached surge peak; E.D.S., end of major detached surge.

The average valley measurements for the Belham Valley in Table 10.2 record the changes in valley characteristics between subsequent DEMs. The Belham Valley has steepened from an average slope of 5.64° in 1995 to 5.98° in 2010, narrowed by 127 m on average, and shallowed by an average of 25 m due to deposition, mainly in the proximal areas (Tyer's Ghaut area). Tyer's Ghaut has more than 30 m of infill in some locations with total volumetric infill of the order of 5.8×10^6 m^3 (Stinton *et al.* 2014).

Pyroclastic flow and ash-cloud surge deposits

Overview

Since the beginning of the eruption, there have been approximately 50 BAFs with volumes $>1 \times 10^6$ m^3 and 15 BAFs with volumes $>5 \times 10^6$ m^3. There are 20 events, ranging in volume from 0.2×10^6 to 210×10^6 m^3, with mapped deposits. Twelve of these mapped flow deposits were chosen for this study (Table 10.3). Only BAFs originating from dome-collapse events or predominantly dome-collapse events were included. Some events were excluded due to lack of separate basal avalanche and ash-cloud surge maps (e.g. 17 September 1996), lack of channelization for much of the flow (no corresponding valley to measure, e.g. 3 August 1997), because they had a major lateral blast component (e.g. 26 December 1997, 3 December 2008) or because a significant portion of the flow entered the sea (e.g. 20 May 2006, 12 July 2003). The 8 January 2010 event was included despite also being associated with a Vulcanian explosion because it exhibited characteristics that were somewhat transitional in nature between typical pumice flows from Vulcanian fountain collapse and typical BAFs. Pumice clasts accounted for only 5 wt% by volume of the deposits and, while an eruption column reached 8.3 km, the PDC was sourced from the dome summit (Cole *et al.* 2014). The 8 January 2007 event may have had similar origins as it also contained minor pumiceous component (Hards *et al.* 2008; Loughlin *et al.* 2010). Furthermore, the morphology of these flow deposits resembled the BAFs from dome-collapse events included in this study. These events also represent the only flows to inundate the Belham Valley, which, from a hazards perspective, is especially important to investigate.

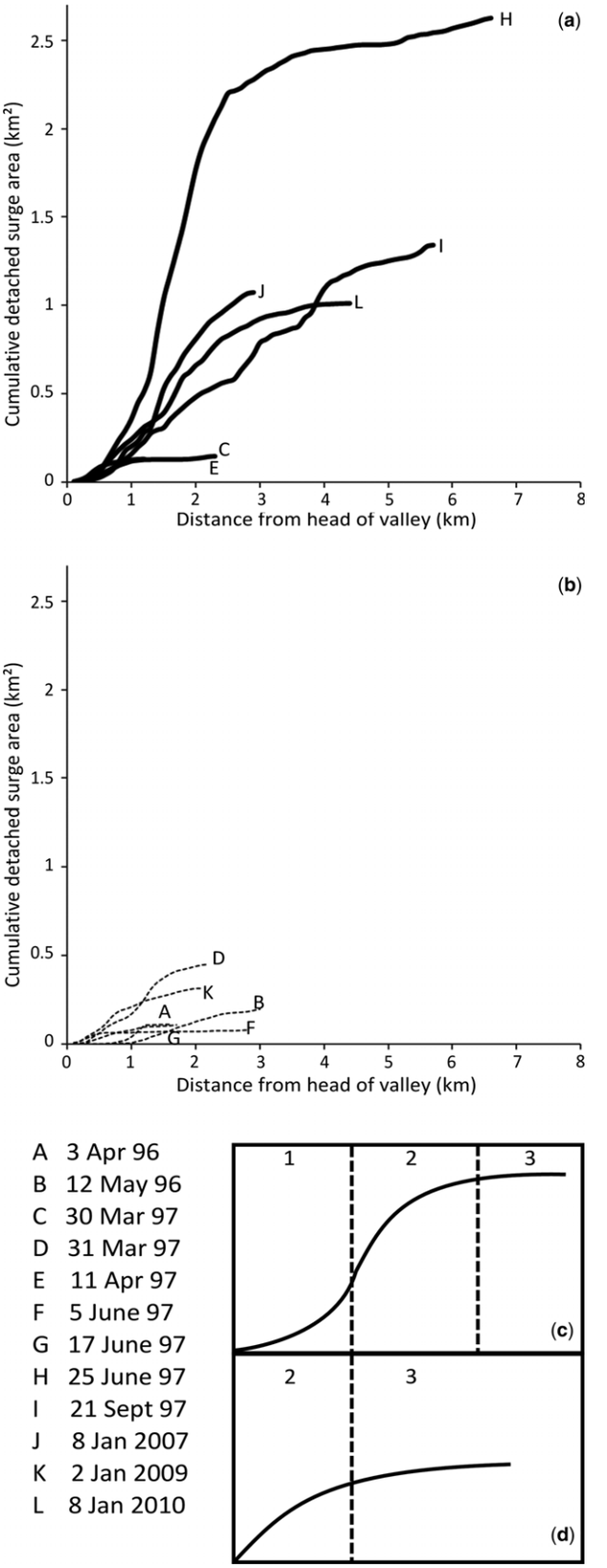

Fig. 10.7. Cumulative detached surge areas for all the BAFs in this study. (**a**) Cumulative detached surge area along-valley for moderate- to large-volume or sustained BAFs. (**b**) Cumulative detached surge area along-valley for small-volume or discrete BAFs. (**c**) Schematic of the cumulative detached surge regions (1, 2, 3) for moderate- to large-volume or sustained BAFs. (**d**) Schematic of the cumulative detached surge regions (2, 3) for small-volume or discrete BAFs;

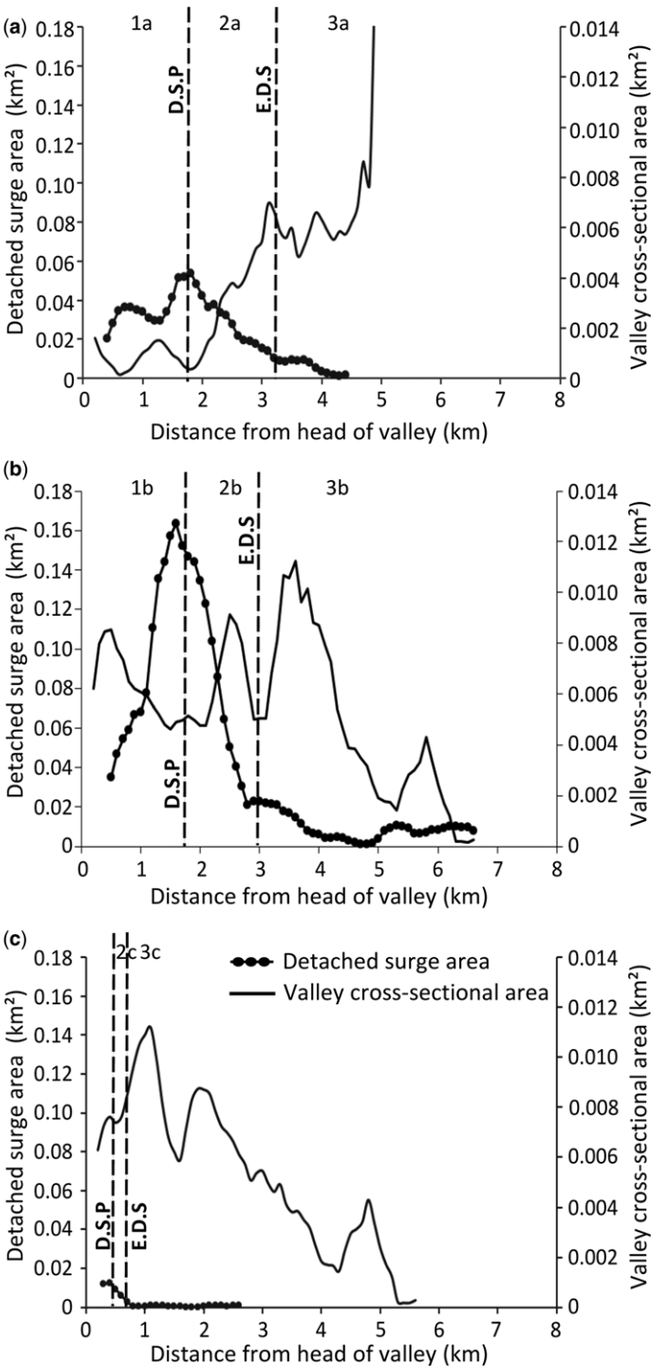

Fig. 10.8. Detached surge area compared with valley cross-sectional area for the (**a**) 8 January 2010 BAF, (**b**) 25 June 1997 BAF and (**c**) 5 June 1997 BAF. D.S.P, detached surge peak; E.D.S, end of major surge detachment. For the large-volume or sustained BAFs (a, b), the sustained surge area is highly negatively correlated with the valley cross-sectional area; that is, the area of detached surge is highest where the valley is narrowest. For small-volume or discrete BAFs (c), the detached surge area is slightly positively correlated with the valley cross-sectional area; that is, the surge spreads to fill the confines of the valley, but does not spill out.

The 25 June 1997 surge-derived flow (while included in the figures herein to avoid distortion of the deposit maps) was not measured as part of the ash-cloud surge, as this part of the flow exhibited a unique generation mechanism and different flow dynamics to the rest of the surge (Druitt *et al.* 2002; Loughlin *et al.* 2002*b*). The 21 September 1997 BAF entered two valleys; most of the

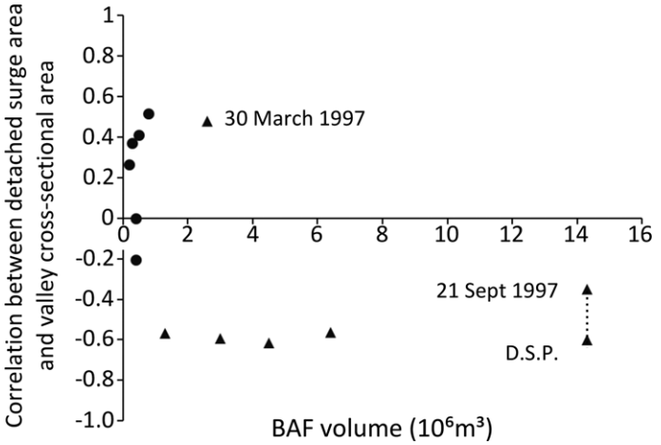

Fig. 10.9. Correlation between detached surge area and valley cross-sectional area compared to the BAF volume. All moderate- to large-volume or sustained BAFs (triangles) show negative correlation, except for the 30 March 1997 flow; all small-volume or discrete BAFs (circles) show a positive correlation. The 21 September 1997 BAF entered more than one valley, the correlation around the detached surge peak (D.S.P.) is therefore also shown.

flow was contained within Tuitt's Ghaut, but some of the BAF entered White's Ghaut. The volume distribution between these valleys is unknown, and BAF measurements were primarily compared to those from Tuitt's Ghaut. Flows from both discrete single-pulse events and sustained dome collapses were included. Discrete events were generally smaller in volume, and consisted of only one pulse or package of flow material (e.g. 5 June 1997). Sustained dome collapses lasted up to 9 h and usually produced large-volume BAFs with many pulses (e.g. 25 June 1997, 21 September 1997).

All the BAFs studied herein are well constrained by volume estimates (with most having separate volume estimates for the dense basal avalanche and the ash-cloud surge components), inundated areas and height/length (H/L) mobility measurements (Table 10.3). Apart from volumes and height dropped, which were extracted from several different sources (Calder *et al.* 1999, 2002; 2010*a*; Hards *et al.* 2008; Loughlin *et al.* 2010), all other values were measured using tools within ArcGIS. Because lengths and areas were measured automatically with GIS tools,

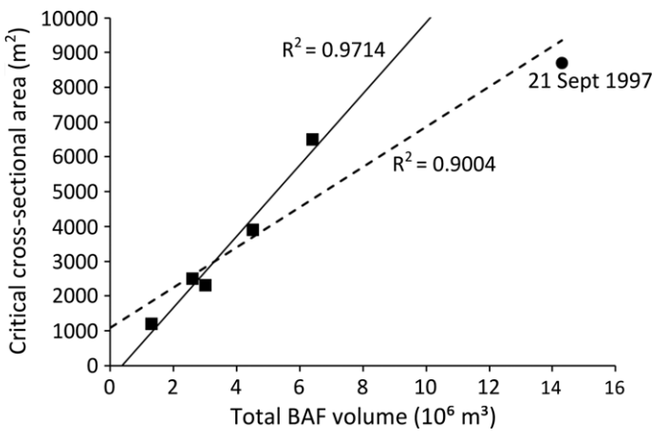

Fig. 10.10. The critical valley cross-sectional area is dependent on BAF volume. When the channel constricts below the critical cross-sectional area, the ash-cloud surge often detaches from the dense basal avalanche. The critical cross-sectional area is approximately 1×10^{-3} of BAF volume. The 21 September 1997 BAF (indicated) entered two valleys, with its volume distributed between the two channels.

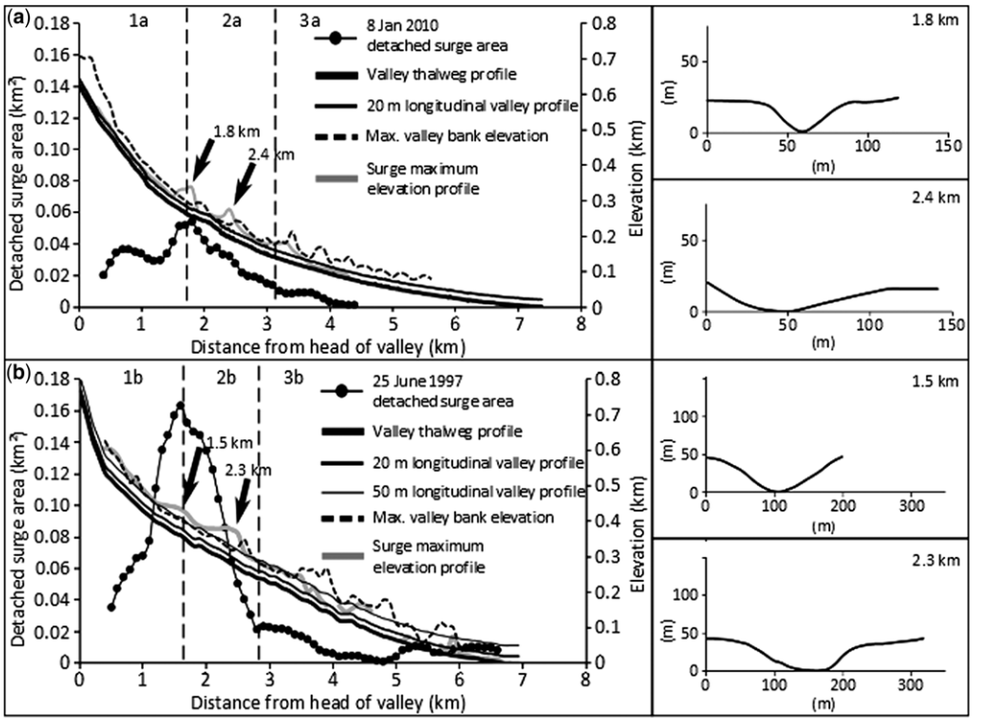

Fig. 10.11. Profile of the maximum elevations traversed by the 8 January 2010 (**a**) and 25 June 1997 (**b**) surges compared with the valley thalweg profile, 20 and 50 m longitudinal-stream profiles, and maximum valley-bank profiles. The highest elevations inundated by the surge are colocated with the maximum detached surge, and also indicate that the surge was not merely filling topography where the peaks in the surge maximum elevation profile exceed the valley bank profiles. Insets show the valley cross-sectional areas at the surge elevation peaks.

they differ slightly from older published values that used other measurement techniques, usually on paper maps. The volume of the BAFs deposits included in this study range from 0.2×10^6 to 14.3×10^6 m^3.

Of critical importance to predicting surge detachment and inundation is the volume partitioning that occurs between the dense basal avalanche and the ash-cloud surge. This partitioning is a complex and poorly understood phenomena that probably depends on many factors, including the explosivity of the eruption, the overpressurization of dome rock, and the size and lithology of the particles involved. Large-volume BAFs do not necessarily produce extensive detached surge deposits (Fig. 10.4a). However, a relationship is observed between the total ash-cloud surge area and the dense basal avalanche volume (Fig. 10.4b); that is, large-volume dense basal avalanches produce ash-cloud surges that cover extensive areas. Voluminous surge clouds are also more likely to detach significantly (Fig. 10.4c). Likewise, dense basal avalanches that cover extensive areas are more likely to have large detached surge areas (Fig. 10.4d). It is therefore difficult to estimate what area might be impacted by a detached surge based only on the BAF collapse volume, but large-volume dense basal avalanches that cover extensive areas are more likely to have ash-cloud surges that detach significantly and cover large areas. This points to possible topographical controls on the detachment of surges, instead of merely volume control.

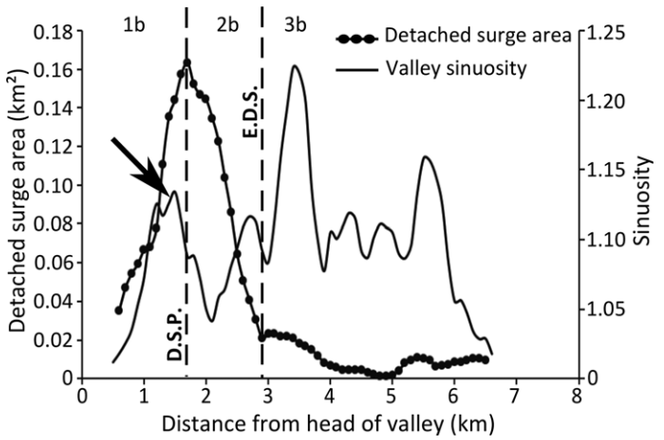

Fig. 10.12. 25 June 1997 detached surge area compared to valley sinuosity. The peak in the detached surge area follows a peak in sinuosity (solid arrow) at a valley bend.

In addition to the measurements in Table 10.3, each deposit was measured along the 100 m-spacing latitudinal profile lines used to measure valley topography. The width of the deposits of the dense basal avalanche and ash-cloud surges were measured at each profile, and respective inundation areas were also measured for each area segment (areas between two consecutive profile lines) (Fig. 10.2). The maximum elevation and average slope (extending laterally away from the valley axis) over which the ash-cloud surge passed was also recorded for each profile. The deposit measurements for all 12 studied deposits were then compared to the cross-channel measurements of the valleys from the appropriate pre-event DEM. For example, the 5 June 1997 deposit measurements were compared to the 10 m DEM of 1995. For illustrative purposes, the relationships found for all studied events are shown in the following figures using only a subset of the events (the 8 January 2010, 25 June 1997 and 5 June 1997 flows), as these provide the clearest examples of the findings discussed throughout.

Deposit morphology

From the ash-cloud surge deposit distributions, several features are immediately apparent. For moderate- to large-volume ($>1 \times 10^6$ m^3) events (which are usually sustained collapses in nature), the data identify three dominant surge regimes: (1) a rapid proximal zone of surge expansion and detachment; (2) a medial deflation zone where the surge extent rapidly diminishes; and (3) a steadier, decaying, distal surge 'fringe' (Fig. 10.5). Proximally (region 1) and medially (region 2), the surge can overspill the channel and spread laterally from the main flow. Alternatively, it

Table 10.4. *Estimated flow-front velocities compared with the TITAN2D modelled maximum velocities*

Date	Valley	Pulse No.	Section (km)	Velocity* ($m\ s^{-1}$)	Error ($m\ s^{-1}$)	Method	TITAN2D velocity ($m\ s^{-1}$)
3 April 1996	TRV		0–2.0	11.0		Seismic	
12 May 1996	TRV	3	0–2.7	7.0	+2.0, −1.0	Video	
		3	2.5–2.7	7.5	+7.5, −0.5	Video	
		3	2.7–2.9	25.0		Video	
31 March 1997	TRV		0–2.0	8.0		Seismic	
5 June 1997	TG		0–1.3	28.0		Video	47.2
			0–2.8	10.0	+1.5, −1	Seismic	28.8
			1.3–2.1	18.5	+1.4, −2.1	Video	18.3
			1.3–2.9	8.2	+0.5, −1.2	Video	12.1
			2.1–2.9	5.5		Video	4.0
25 June 1997	MG	1	0–2.7	31.0	+5, −3	Seismic	
		1	0–3.9	16.7	+1.6, −1.9	Video	56.0
		1	0–4.7	15.0	+1.0, −0.9	Video	41.0
		1	3.9–4.7	10.0	+30, −3	Video	32.0
		2	0–2.7	75.0	+2.9, −2.3	Seismic	35.0
		2	0–4.7	20.2	+1.3, −1.1	Video	60.0
		2	0–6.7	16.1	+15, −8	Video	55.0
		2	4.7–6.7	11.0	+3.2, −2.6	Video	
		3	0–2.7	30.0		Seismic	
		3	0–6.7	21.9		Video	
		3	*c.* 4.4	20.0		SE	
		3	4.4–6.0	8.0		SE	
		Surge	*c.* 3.0	35–37[†]		PE	
		Surge	0–3.0	50–55[†]		DO	
8 January 2010	BV		0–0.4	21.512[‡]	±1.860	Video	39.8
			0.4–1.2	20.833[‡]	±1.042	Video	44.2
			1.2–1.7	19.146[‡]	±1.220	Video	43.6
			1.7–2.7	17.200[‡]	±1.000	Video	38.2
			2.7–2.9	12.353[‡]	±1.765	Video	36.2
			2.9–3.0	11.500[‡]	±1.429	Video	34.6
			3.0–3.3	6.071[‡]	±0.446	Video	32.4
			3.3–3.9	4.636[‡]	±1.136	Video	24.2
			3.9–4.1	4.082[‡]	±1.020	Video	21.2
			4.1–4.4	3.908[‡]	±0.575	Video	10.6

TRV, Tar River Valley; TG, Tuitt's Ghaut; MG, Mosquito Ghaut; BV, Belham Valley, SE, super elevation; PE, potential energy; DO, dynamic overpressure from tree blow-down.

*All velocities are from (Calder 1999) except where noted.

[†]Loughlin *et al.* (2002*b*). This is the velocity of the pyroclastic flow in the corresponding region, not the velocity of the pyroclastic surge.

[‡]Molle (2012).

can detach completely and travel in other quite different directions, as happened on 25 June 1997 (Fig. 10.5b). Region 1 and 2 also correspond to the tree blow-down zone and building damage recorded for some events, which indicate dynamic pressures >7 kPa (Cole *et al.* 2002). Distally (region 3), the surge appears as a narrow fringe adjacent to the dense basal avalanche, and usually remains channelized (e.g. 8 January 2010, Fig. 10.5a), sometimes overtopping channels by a few tens of metres around bends in the channel (e.g. 25 June 1997, Fig. 10.5b). Trees in the distal area remain standing, indicating dynamic pressures <3 kPa (Cole *et al.* 2002).

For small-volume ($<1 \times 10^6$ m^3) or discrete pulse events (e.g. 5 June 1997), there is often a small proximal region (region 2) of surge detachment that persists for a few hundred metres. Distally (region 3), however, the surge deposits are minimal and only detach from the dense basal avalanche around channel bends (Fig. 10.5).

These proximal, medial and distal surge regimes are compared with both peak surge detachment and valley slope in Figure 10.6 for the 8 January 2010 event. On slopes greater than 10° (region 1), surge detachment increases until it reaches peak surge detachment at around 10°; on slopes from 5 to 10° (region 2), the slope detachment decreases until it reaches the beginning of the surge 'fringe' (the distal region) at around 5° (region 3); and on slopes less than 5° (region 3), the surge is present only as a narrow fringe. These relationships are observed for all the moderate- to large-volume events.

The cumulative curves for the detached surge area along the flow path for all the events in this study do show some variations (Fig. 10.7). The first-order distinction between surge development and detachment patterns suggests systematic differences between the moderate- to large-volume or sustained events and the small-volume or discrete events. Moderate- to large-volume events clearly show the three surge regions outlined above, whereas the curves for small-volume events only exhibit the declining surge inundation (region 2) and the distal surge 'fringe' (region 3) (Fig. 10.7).

Valley cross-sectional area

The data show a strong negative correlation between valley cross-sectional area and detached surge area for the 8 January 2010 and

25 June 1997 events (Fig. 10.8a, b); that is, the area of detached surge is greatest where the valley is most constricted. This relationship is observed for all moderate- to large-volume or sustained events (Fig. 10.9), except for the 30 March 1997 BAF in the White River Valley. This flow was the first to inundate the White River Valley, the deepest recorded valley (Table 10.2). Because the 21 September 1997 BAF entered more than one valley, it was more difficult to relate detached surge area to cross-sectional area along the entire length of the flow. For this reason, the area around the detached surge peak was correlated with cross-sectional area and also plotted in Figure 10.9. A critical cross-sectional area can also be identified from this data. The surge detaches from the dense basal avalanche where the valley cross-sectional area falls below 1200 m^2 for the 8 January 2010 BAF and 6800 m^2 for the larger-volume 25 June 1997 BAF. There is a strong correlation between critical cross-sectional area and BAF volume for all moderate- to large-volume BAFs (Fig. 10.10). The critical cross-sectional area is approximately 1×10^{-3} of the BAF volume. The detached surge area from the 5 June 1997 event is either not correlated or is very weakly positively correlated with the valley cross-sectional area (Fig. 10.8c); that is, the surge expands within the valley, but does not spill out. This was the case for all other small-volume events investigated herein (Fig. 10.9).

The extent of topography surmounted by the detached ash-cloud surges is another parameter of interest. Therefore, the maximum elevation that the 8 January 2010 and 25 June 1997 surges surmounted at each latitudinal profile line was determined (Fig. 10.11). This maximum surge elevation profile was then compared with the valley thalweg profile, valley bank profiles, and longitudinal stream profiles (contour lines parallel to the valley thalweg) at 20 and 50 m above the valley thalweg. In essence, the 20 and 50 m contours represent the positions of hypothetical surge clouds with a uniform thickness of 20 or 50 m, if the surge merely filled topography as it descended the drainage. Choosing somewhat arbitrary horizontal or vertical distances from the valley thalweg is a common method of estimating possible surge indunation limits. The difference between the actual maximum surge elevation profile, the maximum valley bank and the longitudinal stream profiles highlights areas where the surge surmounted significant elevation and was not simply infilling topography. For moderate- to large-volume events, the maximum detached surge area is colocated with peaks in surge elevation (Fig. 10.11).

Sinuosity

Detached surge area was also compared to valley sinuosity. Sinuosity was measured at each 100 m-spacing latitudinal profile line, by measuring both the straight-line and along-valley length for the preceding 200 m section. Sinuosity is given as the ratio of the along-valley distance divided by the straight-line distance. The data show a possible relationship between valley sinuosity and the 25 June 1997 detached surge area (Fig. 10.12), and identify a peak in sinuosity preceding the peak detached surge. For many moderate- to large-volume events, there was a possible relationship between peak sinuosity and peak detached surge. The peak in sinuosity (valley bend) either preceded the peak surge detachment by approximately 100 m or coincided with the peak surge detachment. Loughlin *et al.* (2002*b*) identified the same valley bend preceding the detachment of the ash-cloud surge. Comparing sinuosity to deposit metrics was difficult for several reasons: the maximum valley sinuosity (the biggest valley bend) often occurred in more distal regions and did not, therefore, correspond to any changes in surge detachment (i.e. White River Valley events). Many small–moderate BAFs were not mobile enough to encounter these distal valley bends, and large-volume BAFs had probably decelerated to such a degree that even large increases in sinuosity could not produce surge detachment. The effect of sinuosity on surge detachment is, therefore, also highly dependent on other factors such as PDC velocity and thickness. Some valleys did not show appreciable sinuosity (i.e. Tar River Valley).

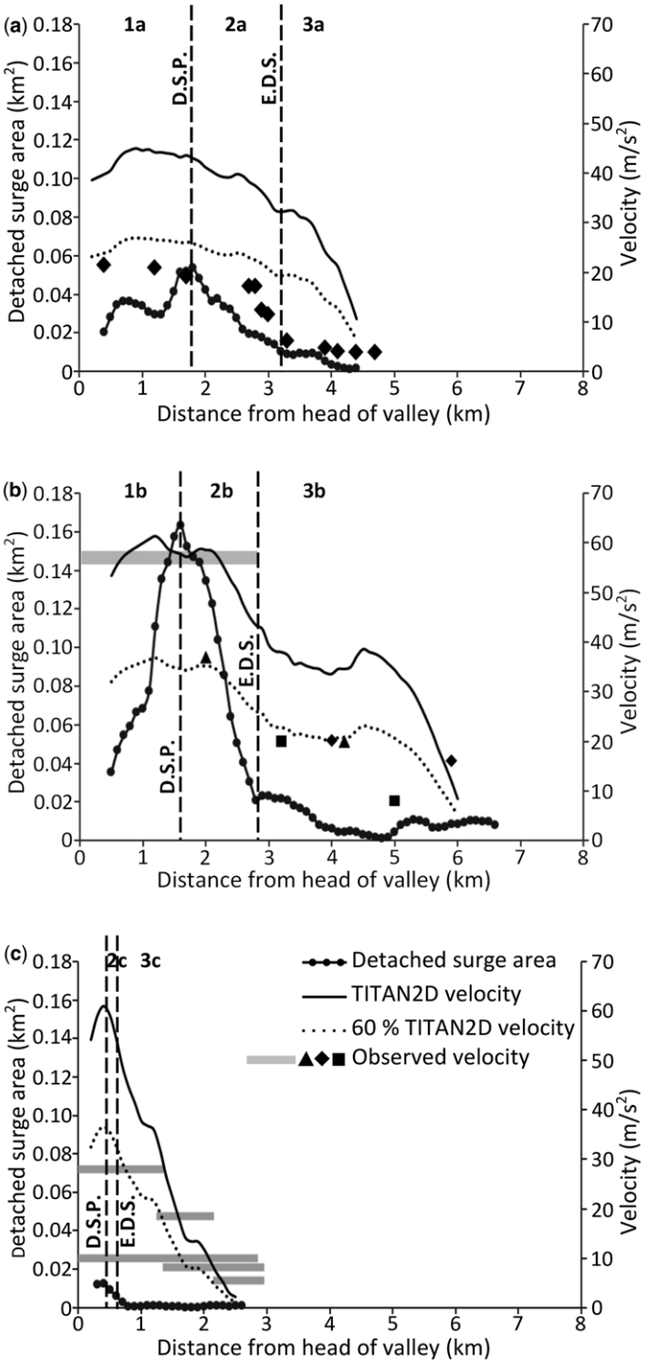

Fig. 10.13. TITAN2D modelled (maximum) dense basal avalanche velocities and observed velocity (flow front) estimates compared with the detached surge area. The dotted lines represent 60% of the modelled maximum velocities for comparison with the estimated flow front velocities. (**a**) The 8 January 2010 detached surge area with observed velocity estimates made from videos of the flow (Molle 2012). (**b**) The 25 June 1997 detached surge area with observed/calculated velocity estimates from Calder (1999) and Loughlin *et al.* (2002*b*). (**c**) The 5 June 1997 detached surge area with observed velocity estimates from Calder (1999). See Table 10.4 for observed velocity specifics, and Table 10.5 for TITAN2D model parameters. Proximal (1), medial (2) and distal (3) flow regimes are noted. D.S.P., detached surge peak; E.D.S., end of major detached surge.

Velocity

Comparing PDC velocity profiles with ash-cloud surge distribution would probably be informative; however, velocity estimates are notoriously difficult to obtain, and exist only for a few events (Table 10.4). In many cases, the velocities are averaged over the entire flow path or averages are obtained for discrete sections of the flow path. The 12 May 1996 event, for instance, has velocity estimates for two 0.2 km sections along the flow path (in addition to a flow path average velocity), but these estimates only occur in the distal regions of the flow, with no estimates of velocity near the peak in ash-cloud surge detachment (Calder 1999). However, a few events have enough data to make useful comparisons (Table 10.4). The 8 January 2010 event has a few preliminary velocity estimates obtained from video analysis (Molle 2012) (Fig. 10.13a); the 25 June 1997 event has several point velocity estimates for the second and third flow pulses, as well as an average estimate of the proximal surge velocity (Loughlin *et al.* 2002*b*) (Fig. 10.13b); and the 5 June 1997 event has several segments with average velocities obtained from video and seismic signal analysis (Calder 1999) (Fig. 10.13c). As seen in Figure 10.13, observed velocity estimates show a strong positive correlation with detached surge area for moderate- to large-volume events. That is, in areas where the dense basal avalanche velocity was at a maximum, the ash-cloud surge was vigorous and spilled out of the valley confines.

Another possibility for comparing flow velocity to ash-cloud surge detachment is to model the dense basal avalanche using a physical flow model and to extract the modelled flow velocities. TITAN2D is a computational model that solves depth-averaged conservation equations for granular flows using a DEM (Patra *et al.* 2005). TITAN2D can use known flow parameters (volume, collapse location and basal friction angles from H/L measurements) to simulate mapped dense basal avalanches. Although TITAN2D does not model the ash-cloud surge, information about how the dense basal avalanche interacts with topography is useful when considering surge dynamics. Using the model, unknowns such as basal avalanche flow thickness, velocity and centre of mass can be approximated. The simulations closely replicate flow volume, centre line and coverage of mapped flows, and also generally agree with the limited data that are known about basal avalanche thickness and velocity. In the absence of other velocity data, or in addition to sparse data, TITAN2D can provide velocity approximations for the entire length of flow runout. Seven flows were modelled using TITAN2D with appropriate input parameters (Table 10.5). The TITAN2D modelled velocities in Figure 10.13 are the *maximum* velocities reached during the simulation at each profile, and show the same general trend in velocity evolution as compared with observed velocity estimates for a number of flows, but there also are considerable differences. In proximal regions, TITAN2D velocities are often tens of m s^{-1} higher than observed velocity estimates (Fig. 10.13a, b). TITAN2D probably overestimates the proximal flow velocities, but, because of poor visibility, it is assumed that proximal observed velocity estimates underestimate actual flow velocities, especially on the upper flanks of the volcano (Loughlin *et al.* 2002*b*). The error estimates in Table 10.4 reflect this, with proximal velocity observations having the largest errors. It is also important to note that the velocities from TITAN2D are *maximum* velocities reached by any part of the flow during the simulation, whereas estimates from observations are *minimum* or *average* flow front velocities. In fact, Simpson (1987) estimated that the flow front travels at only 60% of the maximum speed achieved within the main flow body, which would account for the differences between TITAN2D modelled velocities and observations. Comparing TITAN2D and observed velocities with detached surge areas shows a general positive correlation between velocity and detached surge area (Fig. 10.13), with the highest velocities colocated with the maximum detached surge. Our results show that a line representing 60% of the modelled (maximum) flow velocities correlates well with the estimated flow front velocities. However, TITAN2D does not show all of the variations and peaks in local velocity that observations record because of the differences in measuring maximum flow velocity v. minimum or average flow front local velocities.

Discussion

A number of channel morphology parameters were compared to detached surge areas, including channel slope, width, depth, wetted perimeter, cross-sectional area and sinuosity. Valley width and depth had no consistent correlation with surge detachment, nor did any ratio of width to depth; while slope, wetted perimeter (not discussed as it is related to cross-sectional area, see Fig. 10.2), cross-sectional area and sinuosity all affect surge morphology and detachment. The results here are consistent with the findings of Loughlin *et al.* (2002*b*) for the 25 June 1997 event, of Lube *et al.* (2011) for the June 2006 Merapi BAFs, and of Charbonnier *et al*. (2013) and Komowoski *et al*. (2013) for the October–November 2010 Merapi PDCs, but highlight the extent to which these relationships can be generalized.

The data identify three dominant regimes of surge generation for moderate- to large-volume BAFs: (1) a rapid proximal surge expansion and detachment on slopes greater than 10°; (2) a medial decline in surge expansion after the peak surge detachment on slopes from 5 to 10°; and (3) a more uniform distal surge 'fringe' on slopes less than 5°. Breaks in slope have been proposed as a major driving factor in the development and detachment of surges at Merapi, with significant detachment and decoupling occurring as BAFs flow across the break in slope at the foot of the cone, an area composed of cliffs and a slope that rapidly changes from >30° in the proximal 1.5 km to less than 15° from 1.5 to 2 km (Bourdier & Abdurachman 2001; Charbonnier & Gertisser 2008, 2009, 2011; Lube *et al.* 2011; Jenkins *et al*. 2013). Valley slopes on Montserrat tend to change

Table 10.5. *TITAN2D modelled parameters*

PDC date	Valley	DEM	Simulation volume (10^6 m^3)	Initiation angle (CCW from east = 0°) (°)	Internal friction angle (°)	Basal friction angle (°)
3 April 1996	TRV	Pre-eruption, added dome	0.35	40	25	22
30 March 1997	TRV	Pre-eruption, added dome	2.90	260	25	9
5 June 1997	TG	Pre-eruption, added dome	0.58	80	25	15
25 June 1997	MG	Pre-eruption, added dome	5.54	100	25	8
21 September 1997	TG	Pre-eruption, added dome	12.38	80	25	8
8 January 2007	BV	2007, added dome	4.23	135	25	8
8 January 2010	BV	2010, added dome	1.09	125	25	7

TRV, Tar River Valley; TG, Tuitt's Ghaut; MG, Mosquito Ghaut; BV, Belham Valley.

more gradually, but, even so, there is a general relationship between slope and surge generation and detachment.

An inverse correlation exists between surge detachment and valley cross-sectional area for all moderate- to large-volume BAFs; that is, valley constrictions greatly promote surge detachment. Once a valley constricts below a critical cross-sectional area, surges overspill the channels and inundate large areas. This critical cross-sectional area is, naturally, dependent on the volume (or, more specifically, mass flux) of the BAF; for instance, the critical cross-sectional area is about 1200 m^2 for the 8 January 2010 event and 6800 m^2 for the 25 June 1997 event. In fact, critical cross-sectional area appears to be roughly 1×10^{-3} of BAF volume. Sustained events, consisting of multiple pulses that progressively infill channels and reduce cross-sectional area, are thus most likely to experience significant surge detachment. For hazard-mapping purposes, one could identify critical channel constrictions for a range of BAF volumes in order to predict where ash-cloud surges are likely to overspill the channels. An example of this type of mapping is shown in Figure 10.14. Critical cross-sectional areas were identified for three flow volumes (1×10^6, 5×10^6 and 10×10^6 m^3), and regions of the Belham Valley where this critical cross-sectional area is exceeded were indicated. This information is useful for indicating where ash-cloud surges are likely to detach, and shows that the 'danger area' for surge detachment migrates downstream with larger flows. It is important to note that these examples do not consider flow runout. For example, Figure 10.14c, which maps areas where the critical cross-sectional area is exceeded for a 5×10^6 m^3 volume flow, shows a red zone at the most distal reaches of the Belham Valley. A flow of this size is, however, unlikely to actually reach these areas. Small-volume BAFs show surge detachment only within the first few hundred metres of the flows, which then decreases rapidly, and some minimal surge detachment around valley bends in more distal regions. Valley cross-sectional area plays a minor role in surge detachment for small-volume events where the flows are almost completely contained within the channels.

This negative correlation between valley cross-sectional area and detached surge area makes intuitive sense; surges spill out of narrow or shallow channels and travel laterally, often surmounting steep slopes and gaining elevation. As valleys are progressively in-filled by successive pulses from sustained collapses, the extent of channel overspilling can increase with time through a sustained event. This corresponds with the findings of Loughlin *et al.* (2002*b*), which showed that valley constrictions and depositional filling of channels contributed to the ash-cloud detachment during the 25 June 1997 event. However, comparing the elevations traversed by detached surges with valley-bank and longitudinal-stream profiles shows that the surges are far from simply in-filling topography in the proximal and medial zones (regions 1 and 2). High-velocity surges often surmount steep slopes and gain elevation beyond that which would be expected for a surge of uniform thickness infilling topography. This is especially so at areas of peak surge detachment. This is consistent with experiments by Andrews & Manga (2011), which showed that flows were able to surmount obstructions up to 1.5 times the current thickness, and that barriers less than this height serve to enhance air entrainment and buoyancy. In distal areas (region 3), however, the surges appear as narrow fringes that, to a first order, do fill topography. However, even in distal regions, surges do gain elevation and detach more vigorously at valley bends, which is particularly important for assessing the hazard to communities along the distal reaches of the Belham Valley.

In addition, pyroclastic surge detachment does not seem to be merely a function of BAF volume, although volume certainly plays a role. Surge detachment does seem to have a relationship with surge volume (as opposed to total BAF volume), suggesting that processes that drive surge formation (e.g. elutriation, comminution, entrainment) play a significant role in the decoupling

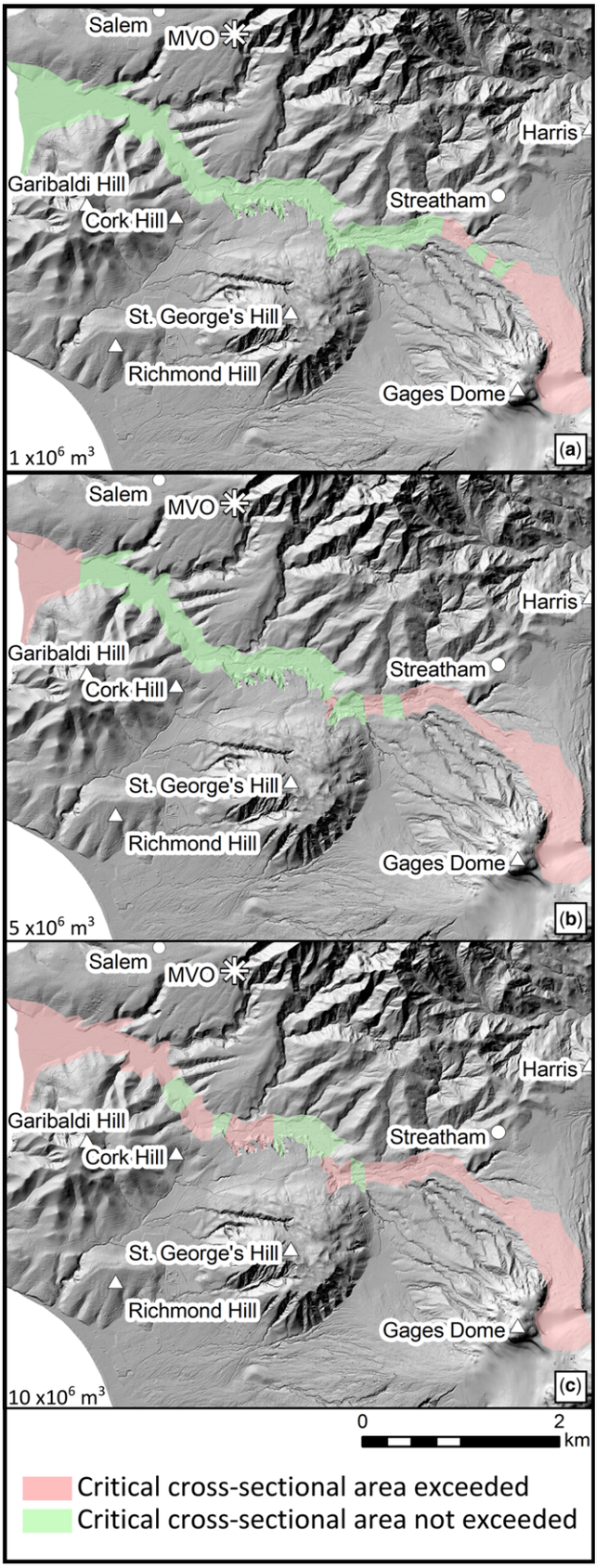

Fig. 10.14. Areas in the Belham Valley where critical cross-sectional areas were exceeded (red areas) for three BAF volumes (1×10^6 (**a**), 5×10^6 (**b**) and 10×10^6 m^3 (**c**)). These maps show an example of how the relationship between BAF volume and critical cross-sectional area could be used for mapping areas where surge detachment is likely.

of pyroclastic surges. We recognize that other factors such as dome pressurization, explosivity, and particle size and lithology may also influence the generation, but detailed investigations of these aspects are beyond the scope of this work. Observational and modeled pyroclastic flow and surge velocities show a correlation with surge detachment. A relationship exists between experimental flow velocity and comminution of ash from pumice blocks (Cagnoli & Manga 2004; Dufek & Manga 2008). Collisions among highly pressurized clasts can release gas and ash, and promote the fluidization of fine particles (Fujii & Nakada 1999). Areas of inferred topography-induced increases in velocity could result in more numerous or vigorous particle collisions, causing more particles to become fluidized, ultimately enhancing surge generation.

From these data, we propose the following conceptual model for ash-cloud surge development and detachment.

Proximally (region 1), vigorous surge expansion is probably due to a combination of high velocities due to steep slopes, and auto-brecciation processes and explosive expansion of pressurized dome rock during collapse. The surge reaches a maximum detached surge area when the valley constricts below a critical, volume-dependent, capacity. Here, passive overflow processes combine with more active velocity- and constriction-induced increases in interparticle collisions to contribute to the vigorous detachment of the surge. After the surge reaches a maximum detachment, the expansion decreases as the valley slope shallows and the valley broadens in the medial region 2. Building damage and tree blow-down in regions 1 and 2 indicate dynamic pressures >7 kPa (Cole *et al.* 2002). Distally (region 3), the ash-cloud surge deposits appear as narrow fringes around the dense basal avalanche deposits, indicative of more passive expansion of elutriated fines from the basal avalanche and subsequent lift-off. In this region, the ash-cloud surges expand to fill topography, sometimes spilling out of channels around valley bends. Damage to trees is minimal, indicating dynamic pressure <3 kPa (Cole *et al.* 2002).

Small-volume flows exhibit only the characteristics of regions 2 and 3. Some surge detachment occurs in the proximal 0.5–1 km, but this appears to be directly related to collapsing dome rock, as the surge expansion declines rapidly from the start of the deposit. In this regard, the proximal surge detachment for small-volume flows resembles region 2, as described above. In region 3, there is minimal surge detachment, only around valley bends. Small-volume events simply fill topography.

Concluding remarks

Relatively few available numerical models attempt to simultaneously capture the behaviour of both the dense and dilute parts of lava dome-collapse PDCs (Denlinger 1987; Fujii & Nakada 1999; Burgisser & Bergantz 2002; Doyle *et al.* 2008). Some simulation tools exist for modelling coupled dense–dilute flows using Lagrangian methods (e.g. Takahashi & Tsujimoto 2000; Todesco *et al.* 2002; Dartevelle *et al.* 2004; Valentine *et al.* 2011), but these models are complex and computationally expensive. Other computational models exist to model the dense basal avalanche (Kelfoun & Druitt 2005; Patra *et al.* 2005; Kelfoun *et al.* 2009) or the ash-cloud surge separately (Ishimine 2005). Simpler empirical models have also shown success (e.g. Wadge *et al.* 1998; Wadge 2000; Widiwijayanti *et al.* 2008), but have similar limitations for modelling both the coupling of the pyroclastic flows and surges. Using these models for hazard mapping can therefore be problematic, as potential surge inundation limits are typically drawn in as a uniform lateral buffer around the modelled dense basal avalanche (e.g. Ogburn 2008; Widiwijayanti *et al.* 2008) or estimated with simple models for lateral motion (e.g. Wadge *et al.* 1998; Wadge 2000; Widiwijayanti *et al.* 2008). The models for lateral motion assume that a uniform percentage (10%) of the dense basal avalanche is elutriated to form the surge, which seems unlikely given the data presented herein. In distal region 3, where the surge exists as a narrow 'fringe' around the dense basal avalanche and generally fills topography by passive lateral expansion, these methods might be reasonable approximations. In fact, we have shown that a 'vertical buffer', determined by calculating longitudinal-stream profiles parallel to the valley thalweg and whose height is based on BAF volume, captures the detached surge area in region 3 quite well. However, horizontal or vertical buffers and 1D models that assume a uniform surge elutriation percentage would not predict the detached surge areas in the proximal and medial regions 1 and 2, where the surge expands rapidly, spills vigorously from constrictions and surmounts steep topography. Here, the surge is not merely filling topography or passively expanding. Instead, the communition of ash and the release of gas from colliding particles of high pore pressure dome rock leads to the generation of violently expanding turbulent ash-cloud surges with capabilities of reaching high lateral velocities. In this region, surge mobility and potential detachment is enhanced by steep slopes, and valley constrictions within region 1 and, to a decreasing degree, region 2.

Characterizing the effect of topography on BAFs can lead to a better understanding of PDC mobility, and ash-cloud surge generation and detachment mechanisms. The relationships investigated herein have the potential to inform physical flow models and to be directly incorporated into empirical models for delineating surge detachment. Improving our ability to accurately gauge zones potentially at risk from surge inundation remains a key concern; indeed, understanding and forecasting surge detachment continues to represent a point of weakness in volcanic hazard mitigation.

Without the dedication of numerous MVO staff, who originally created and compiled many of the deposit maps, this work would not have been possible. E. S. Calder and S. E. Ogburn were supported by NSF grants 0809543 and 0757367.

References

Andrews, B. J. & Manga, M. 2011. Effects of topography on pyroclastic density current runout and formation of coignimbrites. *Geology*, **39**, 1099–1102, http://dx.doi.org/10.1130/G32226.1

Bourdier, J.-L. & Abdurachman, E. K. 2001. Decoupling of small-volume pyroclastic flows and related hazards at Merapi volcano, Indonesia. *Bulletin of Volcanology*, **63**, 309–325, http://dx.doi.org/10.1007/s004450100133

Bullard, F. M. 1962. *Volcanoes in History, in Theory, in Eruption*. University of Texas Press, Austin, TX.

Burgisser, A. & Bergantz, G. W. 2002. Reconciling pyroclastic flow and surge: the multiphase physics of pyroclastic density currents. *Earth and Planetary Science Letters*, **202**, 405–418, http://dx.doi.org/10.1016/S0012-821X(02)00789-6

Calder, E. S. 1999. *Dynamics of small to intermediate volume pyroclastic flows*. PhD thesis, University of Bristol.

Calder, E. S., Cole, P. D., Dade, W. B., Druitt, T. H. & Hoblitt, R. 1999. Mobility of pyroclastic flows and surges at the Soufrière Hills Volcano, Montserrat. *Geophysical Research Letters*, **26**, 537–540, http://dx.doi.org/10.1029/1999GL900051

Cagnoli, B. & Manga, M. 2004. Granular mass flows and Coulomb's friction in shear cell experiments: implications for geophysical flows. *Journal of Geophysical Research*, **109**, F04005, http://dx.doi.org/10.1029/2004JF000177

Charbonnier, S. J. & Gertisser, R. 2008. Field observations and surface characteristics of pristine block-and-ash flow deposits from the 2006 eruption of Merapi Volcano, Java, Indonesia. *Journal of Volcanology and Geothermal Research*, **177**, 971–982, http://dx.doi.org/10.1016/j.volgeores.2008.07.008

Charbonnier, S. & Gertisser, R. 2009. Numerical simulations of block-and-ash flows using the TITAN2D flow model: examples

from Merapi Volcano, Indonesia. *Bulletin of Volcanology*, **71**, 953–959, http://dx.doi.org/10.1007/s00445-009-0299-1

Charbonnier, S. & Gertisser, R. 2011. Deposit architecture and dynamics of the 2006 block-and-ash flows of Merapi Volcano, Java, Indonesia. *Sedimentology*, **58**, 1573–1612, http://dx.doi.org/10.1111/j.1365-3091.2011.01226.x

Charbonnier, S. J., Germa, A. *et al.* 2013. Evaluation of the impact of the 2010 pyroclastic density currents at Merapi volcano from high-resolution satellite imagery, field investigations and numerical simulations. *Journal of Volcanology and Geothermal Research*, **261**, 295–315, http://dx.doi.org/10.1016/j.jvolgeores.2012.12.021

Cole, P. D., Calder, E. S. *et al.* 2002. Deposits from dome-collapse and fountain-collapse pyroclastic flows at Soufrière Hills Volcano, Montserrat. *In*: Druitt, T. H. & Kokelaar, B. P. (eds) *The Eruption of Soufrière Hills Volcano, Montserrat, from 1995 to 1999*. Geological Society, London, Memoirs, **21**, 231–262, http://dx.doi.org/10.1144/GSL.MEM.2002.021.01.11

Cole, P., Bass, V. *et al.* 2010. *Report to the Scientific Advisory Committee on Montserrat Volcanic Activity – Report on Activity between 15 August 2009 and 28 February 2010, Part 1 – Main Report*. Montserrat Volcano Observatory, Open File Report **10-01a 2010**. Montserrat Volcano Observatory, Flemmings, Montserrat.

Cole, P. D., Smith, P. J., Stinton, A. J., Odbert, H. M., Bernstein, M. L., Komorowski, J. C. & Stewart, R. 2014. Vulcanian explosions at Soufrière Hills Volcano, Montserrat between 2008 and 2010. *In*: Wadge, G., Robertson, R. E. A. & Voight, B. (eds) *The Eruption of Soufrière Hills Volcano, Montserrat from 2000 to 2010*. Geological Society, London, Memoirs, **39**, 93–111, http://dx.doi.org/10.1144/M39.5

Darnell, A. R., Lovett, A. A., Barclay, J. & Herd, R. A. 2010. An application-driven approach to terrain model construction. *International Journal of Geographical Information Science*, **24**, 1171–1191, http://dx.doi.org/10.1080/13658810903318889

Dartevelle, S., Rose, W. I., Stix, J., Kelfoun, K. & Vallance, J. W. 2004. Numerical modeling of geophysical granular flows: 2. Computer simulations of plinian clouds and pyroclastic flows and surges. *Geochemistry Geophysics Geosystems*, **5**, 1–36, http://dx.doi.org/10.1029/2003GC000637

Denlinger, R. P. 1987. A model for generation of ash clouds by pyroclastic flows, with application to the 1980 eruptions at Mount St. Helens, Washington. *Journal of Geophysical Research*, **92**, 284–298, http://dx.doi.org/10.1029/JB092iB10p10284

Doyle, E. E., Hogg, A. J., Mader, H. M. & Sparks, R. S. J. 2008. Modeling dense pyroclastic basal flows from collapsing columns. *Geophysical Research Letters*, **35**, 1–5, http://dx.doi.org/10.1029/2007GL032585

Druitt, T. H., Calder, E. S. *et al.* 2002. Small-volume, highly mobile pyroclastic flows formed by rapid sedimentation from pyroclastic surges at Soufrière Hills Volcano, Montserrat: an important volcanic hazard. *In:* Druitt, T. H. & Kokelaar, B. P. (eds) *The Eruption of Soufrière Hills Volcano, Montserrat, from 1995 to 1999*. Geological Society, London, Memoirs, **21**, 211–231, http://dx.doi.org/10.1144/GSL.MEM.2002.021.01.12

Dufek, J. & Manga, M. 2008. In situ production of ash in pyroclastic flows. *Journal of Geophysical Research*, **113**, 1–17, http://dx.doi.org/10.1029/2007JB005555

Fisher, R. V. 1979. Models for pyroclastic surges and pyroclastic flows. *Journal of Volcanology and Geothermal Research*, **6**, 305–318, http://dx.doi.org/10.1016/0377-0273(79)90008-8

Fisher, R. V. 1995. Decoupling of pyroclastic currents: hazards assessments. *Journal of Volcanology and Geothermal Research*, **66**, 257–263, http://dx.doi.org/10.1016/0377-0273(94)00075-R

Fisher, R. V. & Heiken, G. 1982. Mt. Pelée, Martinique: May 8 and 20, 1902, pyroclastic flows and surges. *Journal of Volcanology and Geothermal Research*, **13**, 339–371, http://dx.doi.org/10.1016/0377-0273(82)90056-7

Fujii, T. & Nakada, S. 1999. The 15 September 1991 pyroclastic flows at Unzen Volcano (Japan): a flow model for associated ash-cloud surges. *Journal of Volcanology and Geothermal Research*, **89**, 159–172, http://dx.doi.org/10.1016/S0377-0273(98)00130-9

Hards, V., Strutt, M., De Angelis, S., Ryan, G., Christopher, T., Syers, T. & Bass, V. 2008. *Report to the Scientific Advisory Committee on activity at Soufrière Hills Volcano Montserrat: April 2008*. Montserrat Volcano Observatory, Open File Report **OFR 09-01**. Montserrat Volcano Observatory, Flemmings, Montserrat.

Ishida, M., Hatano, H. & Shirai, T. 1980. The flow of solid particles in an aerated inclined channel. *Powder Technology*, **27**, 7–12, http://dx.doi.org/10.1016/0032-5910(80)85035-2

Ishimine, Y. 2005. Numerical study of pyroclastic surges. *Journal of Volcanology and Geothermal Research*, **139**, 33–57, http://dx.doi.org/10.1016/j.jvolgeores.2004.06.017

Jenkins, S., Komorowski, J.-C., Baxter, P. J., Spence, R., Picquout, A., Lavigne, F. & Surono. 2013. The Merapi 2010 eruption: an interdisciplinary impact assessment methodology for studying pyroclastic density current dynamics. *Journal of Volcanology and Geothermal Research*, **261**, 316–329, http://dx.doi.org/10.1016/j.jvolgeores.2013.02.012

Kelfoun, K. & Druitt, T. H. 2005. Numerical modeling of the emplacement of Socompa rock avalanche, Chile. *Journal of Geophysical Research*, **110**, 1–13, http://dx.doi.org/10.1029/2005JB003758

Kelfoun, K., Samaniego, P., Palacios, P. & Barba, D. 2009. Testing the suitability of frictional behaviour for pyroclastic flow simulation by comparison with a well-constrained eruption at Tungurahua volcano (Ecuador). *Bulletin of Volcanology*, **71**, 1057–1075, http://dx.doi.org/10.1007/s00445-009-0286-6

Kieffer, S. W. 1981. Fluid dynamics of the May 18 blast at Mount St. Helens. *In*: Lipman, P. & Mullineaux, D. (eds) *The 1980 Eruptions of Mount St Helens, Washington*. United States Geological Survey, Professional Paper, **1250**, 379–400.

Komorowski, J.-C., Legendre, Y. *et al.* 2010. Insights into the processes and deposits of hazardous vulcanian explosions at Soufrière Hills Volcano during 2008 and 2009 (Montserrat, West Indies). *Geophysical Research Letters*, **37**, 1–6, http://dx.doi.org/10.1029/2010GL042558

Komorowski, J.-C., Jenkins, S. *et al.* 2013. Paroxysmal dome explosion during the Merapi 2010 eruption: processes and facies relationships of associated high-energy pyroclastic density currents. *Journal of Volcanology and Geophysical Research*, **261**, 260–294, http://dx.doi.org/10.1016/j.jvolgeores.2013.01.007

Lirer, L., Pescatore, T., Booth, B. & Walker, G. P. L. 1973. Two Plinian pumice-fall deposits from Somma-Vesuvius, Italy. *Geological Society of America Bulletin*, **84**, 759–772, http://dx.doi.org/10.1130/0016-7606(1973)84<759:TPPDFS>2.0.CO;2

Loughlin, S. C., Baxter, P. J., Aspinall, W. P., Darroux, B., Harford, C. L. & Miller, A. D. 2002*a*. Eyewitness accounts of the 25 June 1997 pyroclastic flows and surges at Soufrière Hills Volcano, Montserrat, and implications for disaster mitigation. *In*: Druitt, T. H. & Kokelaar, B. P. (eds) *The Eruption of Soufrière Hills Volcano, Montserrat, from 1995 to 1999*. Geological Society, London, Memoirs, **21**, 211–231, http://dx.doi.org/10.1144/GSL.MEM.2002.021.01.10

Loughlin, S. C., Calder, E. S. *et al.* 2002*b*. Pyroclastic flows and surges generated by the 25 June 1997 dome collapse, Soufrière Hills Volcano, Montserrat. *In*: Druitt, T. H. & Kokelaar, B. P. (eds) *The Eruption of Soufrière Hills Volcano, Montserrat, from 1995 to 1999*. Geological Society, London, Memoirs, **21**, 191–209, http://dx.doi.org/10.1144/GSL.MEM.2002.021.01.09

Loughlin, S. C., Luckett, R. *et al.* 2010. An overview of lava dome evolution, dome collapse and cyclicity at Soufrière Hills Volcano, Montserrat, 2005–2007. *Geophysical Research Letters*, **37**, 1–6, http://dx.doi.org/10.1029/2010GL042547

Lube, G., Cronin, S. J., Thouret, J.-C. & Surono. 2011. Kinematic characteristics of pyroclastic density currents at Merapi and controls on their avulsion from natural and engineered channels. *Geological Society of America Bulletin*, **123**, 1127–1140, http://dx.doi.org/10.1130/B30244.1

McTaggart, K. C. 1960. The mobility of nuées ardentes. *American Journal of Science*, **258**, 369–382, http://dx.doi.org/10.2475/ajs.258.5.369

Molle, A. 2012. *Video Analysis of the January 8th 2010 Pyroclastic Flow from Soufrière Hills Volcano (Montserrat): Flow Dynamics and Modeled Evolution*. MS thesis, State University of New York at Buffalo and Université Blaise-Pascal.

Moore, J. G. & Sisson, T. W. 1981. Deposits and effects of the May 18 pyroclastic surge. *In*: Lipman, P. & Mullineaux, D. (eds) *The 1980 Eruptions of Mount St. Helens, Washington*. United States Geological Survey, Professional Paper, **1250**, 421–438.

Nairn, I. A. & Self, S. 1978. Explosive eruptions and pyroclastic avalanches from Ngauruhoe in February 1975. *Journal of Volcanology and Geothermal Research*, **3**, 39–60.

Ogburn, S. E. 2008. *Potential hazards at Soufrière Hills Volcano, Montserrat: northwards-directed dome-collapses and major explosive eruptions*. MS thesis, State University of New York at Buffalo.

Patra, A. K., Bauer, A. C. *et al.* 2005. Parallel adaptive numerical simulation of dry avalanches over natural terrain. *Journal of Volcanology and Geothermal Research*, **139**, 1–21, http://dx.doi.org/10.1016/j.jvolgeores.2004.06.014

Rose, W. I. Jr., Grant, N. K., Hahn, G. A., Lange, I. M., Powell, J. L., Easter, J. & DeGraff, J. M. 1977. The evolution of Santa Maria Volcano, Guatemala. *Journal of Geology*, **85**, 63–87.

SAC 2007. *Assessment of the Hazards and Risks Associated with the Soufrière Hills Volcano. Montserrat: Part II Technical Report. Eighth Report of the Scientific Advisory Committee on Montserrat Volcanic Activity*. Scientific Advisory Committee Technical Report.

SAC 2011. *Assessment of the Hazards and Risks associated with the Soufrière Hills Volcano, Montserrat. Fifteenth Report of the Scientific Advisory Committee on Montserrat Volcanic Activity. Part II*. Scientific Advisory Committee Technical Report.

Sato, H., Fujii, T. & Nakada, S. 1992. Crumbling of dacite dome lava and generation of pyroclastic flows at Unzen volcano. *Nature*, **360**, 664–666, http://dx.doi.org/10.1038/360664a0

Sheridan, M. F., Hubbard, B., Carrasco-Núñez, G. & Siebe, C. 2004. Pyroclastic flow hazard at Volcán Citlaltépetl. *Natural Hazards*, **33**, 209–221, http://dx.doi.org/10.1023/B:NHAZ.0000037028.89829.d1

Sigurdsson, H., Carey, S. N. & Fisher, R. V. 1987. The 1982 eruption of El Chichón Volcano, Mexico (3): physical properties of pyroclastic surges. *Bulletin of Volcanology*, **49**, 467–488.

Simpson, J. E. 1987. *Gravity Currents in the Environment and the Laboratory*. Cambridge University Press, Cambridge.

SMITHSONIAN INSTITUTION 2011. Merapi. *Bulletin of the Global Volcanism Network*, **36**, 2.

Sparks, R. S. J. 1976. Grain size variations in ignimbrites and implications for the transport of pyroclastic flows. *Sedimentology*, **23**, 147–188, http://dx.doi.org/10.1111/j.1365–3091.1976.tb00045.x

Sparks, R. S. J., Wilson, L. & Hulme, G. 1978. Theoretical modeling of the generation, movement, and emplacement of pyroclastic density flows by column collapse. *Journal of Geophysical Research*, **83**, 1727–1739, http://dx.doi.org/10.1029/JB083iB04p01727

Sparks, R. S. J., Barclay, J. *et al.* 2002. Generation of a debris avalanche and violent pyroclastic density current on 26 December (Boxing Day) 1997 at Soufrière Hills Volcano, Montserrat. *In*: Druitt, T. H. & Kokelaar, B. P. (eds) *The Eruption of Soufrière Hills Volcano, Montserrat, from 1995 to 1999*. Geological Society, London, Memoirs, **21**, 409–434, http://dx.doi.org/10.1144/GSL.MEM.2002.021.01.18

Stefanescu, E. R., Bursik, M. I., Cordoba, G., Patra, A. K., Pieri, D. C. & Sheridan, M. F. 2010*a*. Impact of DEM uncertainty on TITAN2D flow model output, Galeras Volcano, Colombia. *In*: Swayne, D. A., Yang, W., Voinov, A. A., Rizzoli, A. & Filatova, F. (eds) *Modelling for Environment's Sake Proceedings of the Fifth Biennial Conference of the International Environmental Modelling, Software Society, Ottawa, Canada*, July 5–8, 2010. International Environmental Modelling and Software Society (iEMSs), Manno, Switzerland, 427.

Stefanescu, E. R., Bursik, M., Dalbey, K., Jones, M., Patra, A. & Pitman, E. 2010*b*. DEM uncertainty and hazard analysis using a geophysical flow model. *In*: Swayne, D. A., Yang, W., Voinov, A. A., Rizzoli, A. & Filatova, F. (eds) *Modelling for Environment's Sake Proceedings of the Fifth Biennial Conference of the International Environmental Modelling, Software Society, Ottawa, Canada*, July 5–8, 2010. International Environmental Modelling and Software Society (iEMSs), Manno, Switzerland, 418.

Stinton, A. J., Cole, P. D., Odbert, H. M., Christopher, T., Avard, G. & Bernstein, M. 2014. Dome growth and valley fill during Phase 5 (8 October 2009–11 February 2010) at the Soufrière Hills Volcano, Montserrat. *In*: Wadge, G., Robertson, R. E. A. & Voight, B. (eds) *The Eruption of Soufrière Hills Volcano, Montserrat from 2000 to 2010*. Geological Society, London, Memoirs, **39**, 113–131, http://dx.doi.org/10.1144/M39.6

Takahashi, T. & Tsujimoto, H. 2000. A mechanical model for Merapi-type pyroclastic flow. *Journal of Volcanology and Geothermal Research*, **98**, 91–115, http://dx.doi.org/10.1016/S0377-0273(99)00193-6

Todesco, M., Neri, A., Esposti, T., Papale, P., Macedonio, G., Santacroce, R. & Longo, A. 2002. Pyroclastic flow hazard assessment at Vesuvius (Italy) by using numerical modeling. I. Large-scale dynamics. *Bulletin of Volcanology*, **64**, 155–177, http://dx.doi.org/10.1007/s00445-001-0189-7

Valentine, G. A. 1987. Stratified flow in pyroclastic surges. *Bulletin of Volcanology*, **49**, 616–630, http://dx.doi.org/10.1007/BF01079967.

Valentine, G. A., Doronzo, D. M., Dellino, P. & de Tullio, M. D. 2011. Effects of volcano profile on dilute pyroclastic density currents: numerical simulations. *Geology*, **39**, 947–950, http://dx.doi.org/10.1130/G31936.1

Voight, B., Constantine, E. K., Siswowidjoyo, R. & Torley, R. 2000. Historical eruptions of Merapi Volcano, Central Java, Indonesia, 1768–1999. *Journal of Volcanology and Geothermal Research*, **100**, 69–138, http://dx.doi.org/10.1016/S0377-0273 (00)00134-7

Voight, B., Komorowski, J.-C. *et al.* 2002. The 26 December (Boxing Day) 1997 sector collapse and debris avalanche at Soufrière Hills Volcano, Montserrat. *In*: Druitt, T. H. & Kokelaar, B. P. (eds) *The Eruption of Soufrière Hills Volcano, Montserrat, from 1995 to 1999*. Geological Society, London, Memoirs, **21**, 409–434, http://dx.doi.org/10.1144/GSL.MEM.2002.021.01.17

Wadge, G. 2000. *A DEM of the volcanic deposits of Soufrière Hills Volcano during 1999*. Montserrat Volcano Observatory, Open File Report **OFR 00-07**. Montserrat Volcano Observatory, Flemmings, Montserrat.

Wadge, G. 2009. Assessing the pyroclastic flow hazards from dome collapse at Soufrière Hills Volcano, Montserrat. *In*: Thordarson, T., Self, S., Larsen, G., Rowland, S. K. & Hoskuldsson, A. (eds) *Studies in Volcanology: The Legacy of George Walker*. IAVCEI, Special Publications, **2**, Geological Society, London, 211–224.

Wadge, G. & Isaacs, M. C. 1988. Mapping the volcanic hazards from Soufrière Hills Volcano, Montserrat, West Indies using an image processor. *Journal of the Geological Society, London*, **145**, 541–551, http://dx.doi.org/10.1144/gsjgs.145.4.0541

Wadge, G., Jackson, P., Bower, S. M., Woods, A. W. & Calder, E. S. 1998. Computer simulations of pyroclastic flows from dome collapse. *Geophysical Research Letters*, **25**, 3677–3680, http://dx.doi.org/0094-8534/98/98GL-00710

Widiwijayanti, C., Voight, B., Hidayat, D. & Schilling, S. 2008. Objective rapid delineation of areas at risk from block-and-ash pyroclastic flows and surges. *Bulletin of Volcanology*, **71**, 687–703, http://dx.doi.org/10.1007/s00445-008-0254-6

Wilson, C. J. N. 1980. The role of fluidization in the emplacement of pyroclastic claws: an experimental approach. *Journal of Volcanology and Geothermal Research*, **8**, 231–249, http://dx.doi.org/10.1016/0377-0273(80)90106-7

Wilson, C. J. N. & Walker, G. P. L. 1982. Ignimbrite depositional facies: the anatomy of a pyroclastic flow. *Journal of the Geological Society, London*, **139**, 581–592, http://dx.doi.org/10.1144/gsjgs.139.5.0581

Woods, A. W., Sparks, R. S. J., Ritchie, L. J., Batey, J., Gladstone, C. & Bursik, M. I. 2002. The explosive decompression of a pressurized volcanic dome: the 26 December 1997 collapse and explosion of Soufrière Hills Volcano, Montserrat. *In:* Druitt, T. H. & Kokelaar, B. P. (eds) *The eruption of Soufrière Hills Volcano, Montserrat, from 1995 to 1999*. Geological Society, London, Memoirs, **21**, 457–465, http://dx.doi.org/10.1144/GSL.MEM.2002.021.01.20

Yamamoto, T., Takarada, S. & Suto, S. 1993. Pyroclastic flows from the 1991 eruption of Unzen volcano, Japan. *Bulletin of Volcanology*, **55**, 166–175, http://dx.doi.org/10.1007/BF00301514